
Article:
Neehall, N.D., Ismail, M.S. orcid.org/0000-0002-9539-8925, Hughes, K.J. orcid.org/0000-0002-5273-6998 et al. (1 more author) (2021) Effect of composition and structure of gas diffusion layer and microporous layer on the through-plane gas permeability of PEFC porous media. International Journal of Energy Research, 45 (15). pp. 20988-21005. ISSN 0363-907X

https://doi.org/10.1002/er.7158

Title Page

Title

Effect of composition and structure of gas diffusion layer and microporous layer on the through-plane gas permeability of PEFC porous media

Authors

N.D. Neehall, M.S. Ismail, K.J. Hughes *, M. Pourkashanian

Energy 2050, Department of Mechanical Engineering, Faculty of Engineering, University of Sheffield, Sheffield S3 7RD, United Kingdom.

* Corresponding author: Tel: +44 (0) 114 21 57214

Email address: K.J.Hughes@sheffield.ac.uk (K.J. Hughes)

Abstract

The through-plane permeability of the gas diffusion media (GDM) is investigated experimentally with regard to the microporous layer (MPL) composition and the gas diffusion layer (GDL) composition and structure. The MPL composition is held constant at 80% carbon powder and 20% PTFE (by weight) for various carbon loadings. The decrease or increase in GDM permeability was found to be dependent on the structure of the GDL used in conjunction with the type of carbon powder. It was found that a low surface area carbon powder (Vulcan XC-72R) forms thin, dense MPLs with small cracks when compared to a high surface area powder (Ketjenblack EC-300J) which creates thick, rough MPLs with large cracks with increased carbon loadings. For most cases, the permeability decreases with increasing carbon loading; however, the non-woven, straight fibre carbon papers using Ketjenblack EC-300J show the lowest permeability at the lowest carbon loading. Furthermore, the percentage reduction from the GDL substrate permeability appears to be predictable for similar structures with increasing carbon loading. The increase in PTFE loading from 10-30% in the GDL was shown to have a significant impact on the percentage reduction from the original GDL permeability of ~9-15% for GDMs composed of Vulcan XC-72R as a carbon powder; however, such effects are insignificant when using Ketjenblack EC-300J carbon powder.

Keywords: PEFCs; GDLs; MPL; Gas permeability; Carbon loading; GDL structure.

Nomenclature

Italic symbols

D	Circular diameter	m
k	Permeability	m^2
L	Thickness	m
Q	Volumetric flow rate	$m^3 s^{-1}$
u	Velocity	$m s^{-1}$

Greek Symbols

μ	Fluid viscosity	Pa s

Abbreviations

CL	Catalyst layer
FFP	Flow-field plate
GDM	Gas diffusion media (GDL + MPL)
GDL	Gas diffusion layer
MPL	Microporous layer
PEFC	Polymer electrolyte fuel cell
SLPM	Standard litre per minute

1. Introduction

Polymer electrolyte fuel cells (PEFCs) are a promising alternative to the fossil fuel-based, conventional power-generation technologies for portable, automotive and stationary applications due to their ability to exhibit high power densities with rapid, low-temperature start-up and size flexibility [1]–[11]. PEFC components need to demonstrate high transport properties whilst maintaining proper water and thermal management within the cell to achieve these desirable properties. The gas diffusion media (GDM) forms a crucial link between the thermal and water management and the electrochemical activity in the PEFC [4], [6]. The GDM typically consists of a gas diffusion layer (GDL) attached to a microporous layer (MPL) with the GDL situated nearer to the flow-field plate (FFP) and the MPL adjacent to the catalyst layer (CL). The main functions of the GDM are to distribute the reactant gases uniformly and efficiently to the CL, improve the electrical contact with the CL, allow the flow of electrons and heat, and facilitate the removal of excess liquid water away from the electrodes to the flow channels [1], [6], [12].

GDM fabrication typically describes the altering of the GDL substrate by the addition of a hydrophobic material such as PTFE or the addition of a thin layer referred to as an MPL which consists of carbon powder and a binding/hydrophobic agent such as PTFE followed by a heat treatment step. The physical properties of this thin layer are determined from the type, loading and particle size of the carbon powder used in conjunction with the type of hydrophobic agent, such that, the former controls the surface morphology and the later the pore properties [13].

There are numerous studies in the literature which focus on the effects of MPL composition [14-34] aimed at improving the performance of the fuel cell [14-18][20-34]. Furthermore, there are many investigations on the MPL which can be characterized by the type and loading of the hydrophobic agent used [1][14][15][19-24][31] and the carbon powder type used [1][15-19][25-30][32]. Gas permeability is one of the key properties of the PEFC porous media which

describes how effective the convective gas transport is within the porous regions of the fuel cell and accurate values of permeability are needed to obtain realistic saturation profiles in PEFC models [1], [19]. Gas permeability is usually measured in the through-plane or in-plane directions due to the anisotropy of the GDM, that is, in a direction traverse to or orthogonal to the GDM respectively [3]. The investigations presented in this paper focus on the through-plane gas permeability. There have been several experimental investigations into the gas permeability of the PEFC porous layers [1], [3], [19], [35-52]; however, very few [1], [19] have looked at the effect of MPL composition on through-plane gas permeability.

Orogebemi et al. [1] showed the lowest through-plane permeability at 20% PTFE loading for carbon loadings within the range of 0.5-2.5 mg cm^{-2} using Ketjenblack EC-300J carbon powder; an increase in permeability between 20-50% PTFE loading in the MPL was also shown which agreed with the results presented in [3], [40]. Additionally, the through-plane permeability of the GDM using two different carbon powders (Vulcan XC-72R and Ketjenblack EC-300J) was investigated in [19] for a 20% PTFE loading in the MPL for similar carbon loadings. The results indicated a decrease in through-plane permeability with increased carbon loading for the two carbon powders, with the permeability of the GDMs coated with Vulcan XC-72R being higher for carbon loadings less than 1.5 mg cm^{-2}. The investigations conducted by Orogbemi et al. [1], [19] were based on a single GDL substrate, SGL 10BA; however, non-woven carbon fibre commercial GDL substrates differ in structural configurations, namely straight non-woven or felt/'spaghetti' [49] and were not considered in [1], [19].

Most of the cited literature have focused on the through-plane gas permeability of commercial GDL or GDM substrates with the exception of the works conducted by Orogbemi et al. [1], [19] in which GDMs were prepared using a single commercial GDL substrate to investigate the impact of carbon and PTFE loadings in the MPL on through-plane gas permeability. To the

best of the author's knowledge, there have been no previous investigations on the impact of GDL structure (straight non-woven and felt/'spaghetti' carbon fibre paper) and the effects of PTFE loading in the GDL on the through-plane gas permeability of GDMs prepared for different carbon loadings. The focus of this paper extends the works conducted in [1], [19], to include for the first time, the impact of different GDL substrates varying in structure and PTFE composition on GDMs prepared using two different carbon powders, namely, Vulcan XC-72R and Ketjenblack EC-300J. These carbon powders are used for various carbon loadings and the impact on the through-plane gas permeability and thickness of the prepared GDMs before and after application of an MPL were investigated. SEM images were used to investigate surface morphology and MPL thickness. It should be noted that impact of conventional sintering would be discussed in future works and the results reported here were to determine explicitly the impact of the base GDL structure on GDM permeability and morphology of the GDM.

2. Materials and Methods

2.1 Materials

Five different commercial carbon substrates (GDLs) with varying structures were used to prepare the GDM; the manufacturer's data (SGL Carbon GmbH, Meitingen, Germany and Toray International, UK) for these substrates are listed in ***Table 1***. The through-plane gas permeability was investigated for six samples of each GDM. Three carbon loadings of 0.5, 1.0 and 2.0 mg cm^{-2}, utilising two different carbon powders- Vulcan XC-72R (Cabot Corporation, USA) and Ketjenblack EC-300J (AkzoNobel, the Netherlands)- were used to prepare the MPL on each GDL. The manufacturer's data for the carbon powders are given in ***Table 1***.

Table 1. Manufacturers' data for the GDLs and carbon powders.

Properties	Gas Diffusion Layer				
	Straight fibre non-woven			Felt/'spaghetti'	
	Toray TGP-H-120	Toray TGP-H-90	SGL 35BA	SGL 10CA	SGL 10EA
Thickness (µm)	370	280	300	400	374
Areal Weight (g m^{-2})	-	-	54	90	112.9
Porosity (%)	78	78	-	-	-
PTFE Loading (%)	5	5	5	10	30

Properties	Carbon Powder	
	Ketjenblack EC-300J	Vulcan XC-72R
Pore volume (ml/100 g)	310 - 345	178
Apparent bulk density (kg m^{-3})	125 - 145	20 - 380
Surface area (m^2 g^{-1})	950	254
Particle diameter (nm)	30	30
pH	9.0 - 10.5	2 - 11
Volatile (by weight % max.)	1.0	2 - 8

Two other materials apart from the carbon powders were necessary in the preparation of the MPL. A binding agent was necessary to hold the particles together. Polytetrafluorethylene (PTFE) was used as the hydrophobic binding agent - PTFE with 60 wt. % aqueous dispersion emulsion (Sigma Aldrich, UK) was used. Isopropanol (W292907-8KG-K, Sigma Aldrich, UK) was used as a dispersant for the mixture with a ≥ 99.7% concentration. These three materials, that is, carbon black powder, PTFE and isopropanol were used in the preparation of the MPL ink slurry to be coated onto the GDLs as described in Section 2.2.

2.2 Methods

GDL samples were cut from the master sheets using a circular paper punch with a 1-inch diameter [1], [3], [19], [36]. It should be noted that all GDLs used in the investigations conducted in this paper were from the same master sheet except for eight samples of SGL 10EA which were cut from a different master sheet. The thickness of the samples was measured at four equally spaced locations using a micrometre to provide an average thickness of the samples. Prior to application of the MPL, the permeability of the GDL was determined. The experimental setup used to measure the through-plane gas permeability of the GDLs and GDMs was used in the experimental investigations conducted in [1], [3], [19], [36]. ***Figure 1*** shows a schematic representation of the experimental setup. The in-house experimental setup consists of an upper and lower fixture used to facilitate the nitrogen gas flow through the sample, which is positioned between the fixtures as discussed in [36]. It should be noted that the gas permeability is an intrinsic property of the material and is not sensitive to type of gas used.

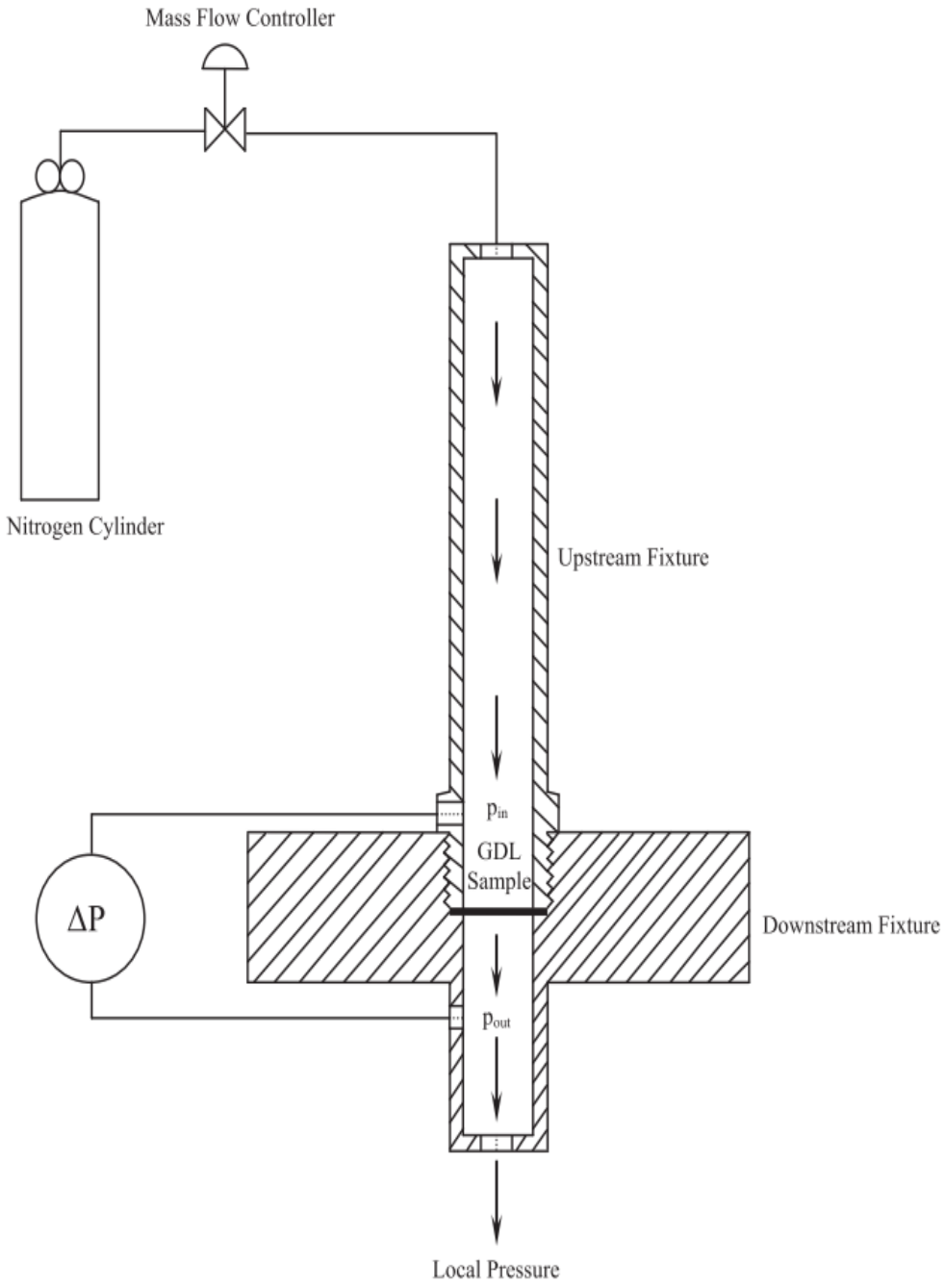

146

147

148 ***Figure 1. Schematic representation of the experimental setup used to measure the through-plane gas permeability.***
149 ***Reprinted from [3] with permission from Elsevier.***

150

151 Eight equally spaced flow rates controlled by a flow controller (HFC-202 Teledyne Hastings,

152 UK) with a range of 0.0 to 0.5 SLPM were used in conjunction with a differential pressure

153 sensor (PX 653 Omega, UK) with a range of ± 12.5 Pa, to determine the pressure drop across
154 the samples.

155 The process of applying an MPL to the GDL using a microporous layer ink slurry was adopted
156 from [1], [19]. The procedure was used here to create an MPL with three different carbon
157 loadings: 0.5, 1.0 and 2.0 mg cm^{-2}. The composition of carbon powder to PTFE was kept
158 constant such that the mixture contained 80 wt. % carbon and 20 wt. % PTFE for all carbon
159 loadings. The necessary amount of carbon powder to PTFE dispersion was determined for the
160 constant composition and manually mixed into a paste. The dispersion agent, isopropanol, was
161 added to the paste and the mixture sonicated for three hours in an ultrasonic bath (U300H,
162 Ultrawave Ltd., UK). The GDLs samples were then mounted onto a heating plate, which was
163 set at a temperature of 80 °C, necessary to evaporate the volatile components of the ink, which
164 was applied to the substrates using a spray gun (Badger 100^{TM} LG, USA). Nitrogen gas was
165 used in the application of the ink onto the GDLs. The permeability of the GDMs was then
166 determined in a similar manner to that of the GDL substrates. It should be noted that the
167 pressure difference values, for the 1.0 and 2.0 mg cm^{-2} carbon loadings for the straight non-
168 woven carbon fibre papers coated with Vulcan XC-72R, exceeded the range of the pressure
169 sensor (±12.5 Pa) used and as such eight equally spaced lower flow rates were used in the
170 determination of the through-plane gas permeability. SEM images were used to determine the
171 surface morphology before and after coating. The model of the scanning electron microscope
172 used was JEOL JSM-6010LA.

173

174

175

2.3 Data analysis

At low fluid velocities (with Reynolds number less than or equal to 3), the viscous resistance to fluid flow was the major cause of the pressure gradient across the porous media for single-phase gas flow due to negligible inertial losses. As such, Darcy's Law was utilised to solve the permeability as follows [1][11][19]:

$$\frac{\Delta P_g}{L} = \frac{\mu_g}{k_g} u_g \tag{1}$$

where u_g is the superficial gas velocity, k_g is the gas-phase permeability, $\mu_g$is the gas-phase dynamic viscosity, ΔP_g is the gas-phase pressure drop and L is the thickness of the sample. Further to this, u_g can be determined as follow:

$$u_g = \frac{Q}{\pi \frac{D^2}{4}} \tag{2}$$

where Q is the volumetric flow rate and D is the diameter of the sample exposed to gas flow [1], [19]. The gas permeability of the bare carbon substrates was determined by curve fitting the experimental data of the pressure gradient across the substrate to the fluid velocity to Eq. (1).

Six samples are used to minimise uncertainties in the permeability measurements carried out in this study and the average permeability plotted with error bars, which represented a 95% confidence interval around the mean.

3. Results and Discussion

3.1 Through-plane gas permeability of the GDLs

Table 2 shows the through-plane permeability and thickness values of all uncoated GDL substrates, before the application of an MPL onto the GDL substrate. The listed values represent the mean and 95% confidence interval limits for the gas permeability and thickness of thirty-six samples per GDL substrate (eighteen samples per each carbon powder). Gas permeability was estimated experimentally by fitting the data, determined from the dependence of fluid velocity on pressure drop, to Equation 1. ***Figure 2*** illustrates the relationship between the pressure gradient across the substrates to the fluid velocity used in the estimation of the gas permeability of the samples. The linearity of the pressure gradient to fluid velocity relationship for the samples investigated justified the use of Darcy's law.

Table 2. Through-plane permeability of tested GDL substrates.

GDL substrates	**Permeability** $k \times 10^{-12}$ $(\mathbf{m^2})$	**Thickness (µm)**
Toray TGP-H-120	5.70 ± 0.13	358.33 ± 1.83
Toray TGP-H-90	6.91 ± 0.13	291.18 ± 0.84
SGL 35BA	39.87 ± 0.80	294.55 ± 1.69
SGL 10CA	21.86 ± 0.46	353.75 ± 5.21
SGL 10EA	18.77 ± 0.97	376.35 ± 6.43

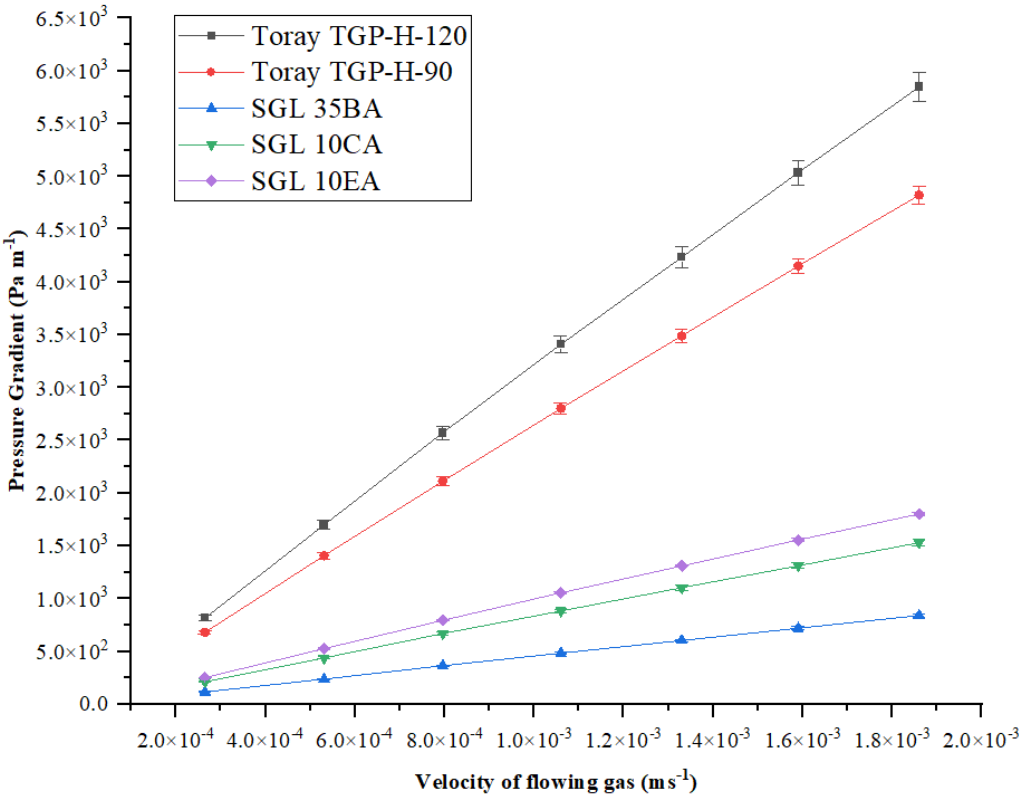

205

206 ***Figure 2. Experimental data for the pressure gradient as a function of fluid velocity for the GDL substrates used.***

207

208 Comparison of the through-plane permeability of the GDL substrates to the available literature
209 shows good agreement. Ismail et al. [36] measured the through-plane permeability of SGL
210 10CA (10% PTFE) and SGL 10EA (30% PTFE) to be 20.3×10^{-12} m^2 and 21.7×10^{-12}
211 m^2 respectively without considering the compressibility of air. Previous studies [40], [42], [43]
212 have shown a decrease in through-plane permeability with an increase in the amount of PTFE
213 and this was due to the partial occupation of the pores by the PTFE particles which
214 subsequently leads to a reduction in the porosity of the medium. This trend is reiterated in the
215 present study. It should be noted that eight of the SGL 10EA samples used in this study were
216 cut from a different sheet and showed through-plane permeability within the range $21.4 -$
217 25.1×10^{-12} m^2. This emphasizes the variability of samples between different sheets, which
218 may be a result of fabrication uncertainties as suggested in [53]. Gostick et al. [48] reported a
219 value of 8.99×10^{-12} m^2 for Toray TGP-H-90 and Mangal et al. [47] reported a value of $8 \times$

10^{-12} m^2 for Toray TGP-H-90 in the through-plane direction for samples with 0% PTFE compared to the 5% PTFE loading in the samples used in this investigation which would probably explain the reduction in permeability as shown in ***Table 2***. Aldakheel et al. [52] reported the through-plane gas permeability of Toray TGP-H-90 with 5% PTFE loading to be 6.62×10^{-12} m^2. Unsworth et al. [54] reported that there is a common misconception of Toray GDLs sharing a uniform microstructure, independent of manufactured thickness; however, based upon through-plane porosity distributions of Toray TGP-H-60 and Toray TGP-H-120 it was shown that the latter was formed through compression of two plies of the former. Similarly, Toray TGP-H-90 was believed to comprise of three plies of Toray TGP-H-30 and as such, it is expected that the permeability values reported in this work should be different between the Toray TGP-H-90 and Toray TGP-H-120 [55]. Williams et al. [37] measured the through-plane permeability of Toray TGP-H-120 and obtained a value of 8.69×10^{-12} m^2. El-Kharouf et al. [49] reported values of 4.53×10^{-12} m^2, 3.90×10^{-12} m^2 and 53.1×10^{-12} m^2 for Toray TGP-H-090, Toray TGP-H-120 and SGL 35BA respectively. Notably, the values obtained in [49] were obtained using a mercury intrusion method (MIP) and therefore it incorporates both the through-plane and in-plane permeability, and as such, should be lower than the values determined here. SGL 35BA shares a similar structure to that of Toray TGP-H-090 and Toray TGP-H-120; all three (3) substrates are categorized in [49] as non-woven carbon papers with straight fibres. The significant difference in through-plane permeability was due to increased porosity due to lower bulk density and increased pore diameters of the SGL 35BA samples [49]. ***Figure 3*** shows the SEM images of the base carbon substrates used in this study. The SEM images of Toray TGP-H-120 and Toray TGP-H-90, shown in Figure 3 (a) and (b) respectively, are very similar which is reflected in the magnitude of the gas permeability; however, it is clear from Figure 3 (c) that the pore sizes are larger for SGL 35BA when compared with those of Toray TGP-H-90 and Toray TGP-H-120 which would explain the

higher gas permeability. Figure 3 (d) and (e) shown are also very similar which would explain the similar magnitudes of gas permeability for SGL 10CA and SGL 10EA even though the PTFE content varied from 10% to 30%.

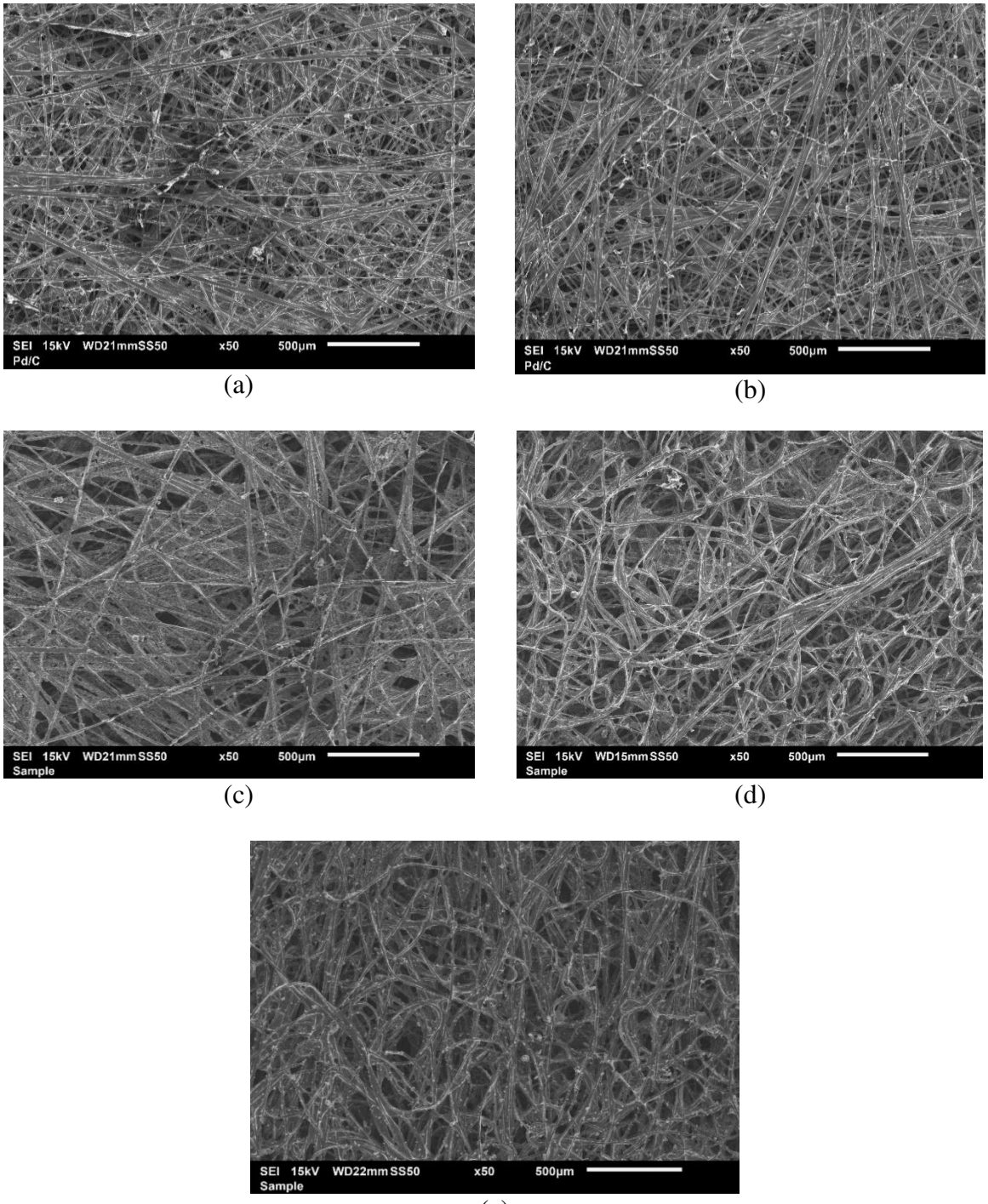

Figure 3. SEM micrographs for (a) Toray TGP-H-120, (b) Toray TGP-H-090, (c) SGL 35BA, (d) SGL 10CA and (e) SGL 10EA.

3.2 Through-plane gas permeability of the Gas diffusion media.

The through-plane gas permeability of GDMs was investigated in this section for two carbon black types, namely Vulcan XC-72R and Ketjenblack EC-300J. The MPL composed of 20% PTFE and 80% carbon black by weight, which was held constant for three carbon loadings: 0.5 mg cm^{-2}, 1.0 mg cm^{-2} and 2.0 mg cm^{-2}. MPL composition values between this range have been widely used in previous studies in the literature namely [19], [56], [57]. Gas permeability of the GDMs was calculated in a similar way to that of the bare substrates with the use of Equation 1. ***Figure 4*** shows the typical pressure gradient as a function of fluid velocity for the GDMs composed of Vulcan XC-72R and Ketjenblack EC-300J MPLs for the two different structured GDLs under investigation, namely: Toray TGP-H-120 and SGL 10EA. The pressure gradient versus velocity curves for the GDMs using Toray TGP-H-90, SGL 35BA and SGL 10CA substrates showed similar linearity (Refer to F-1 of the supplementary material). The error bars represent the 95% confidence interval about the mean.

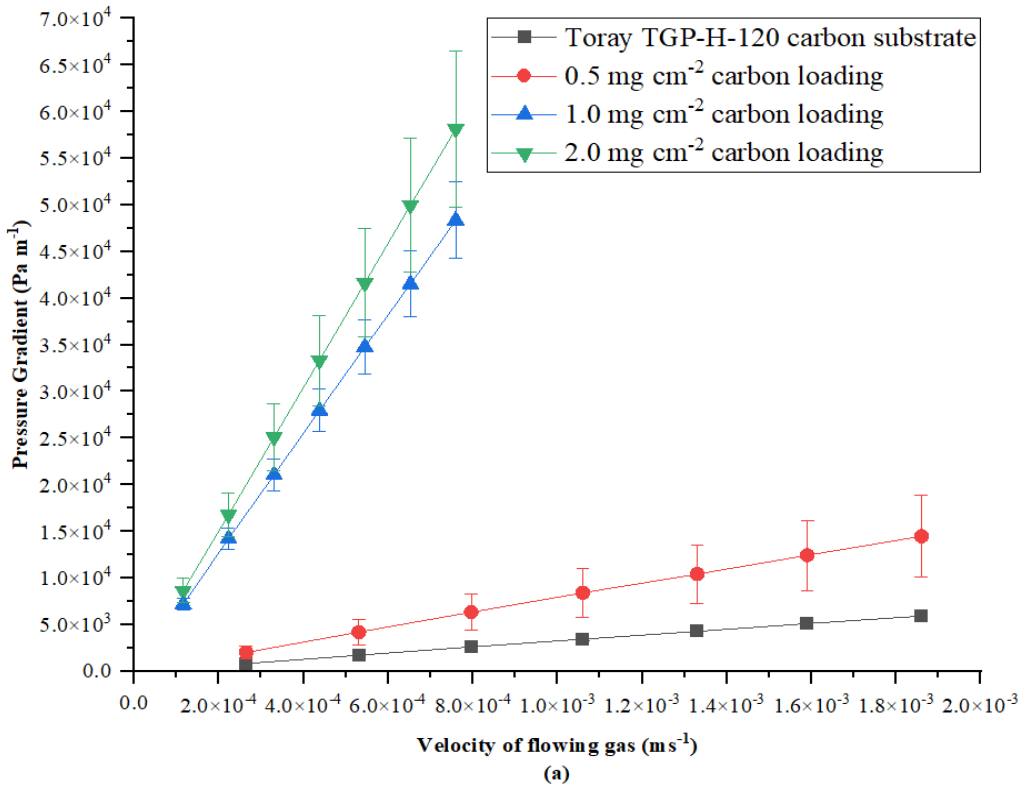

(a)

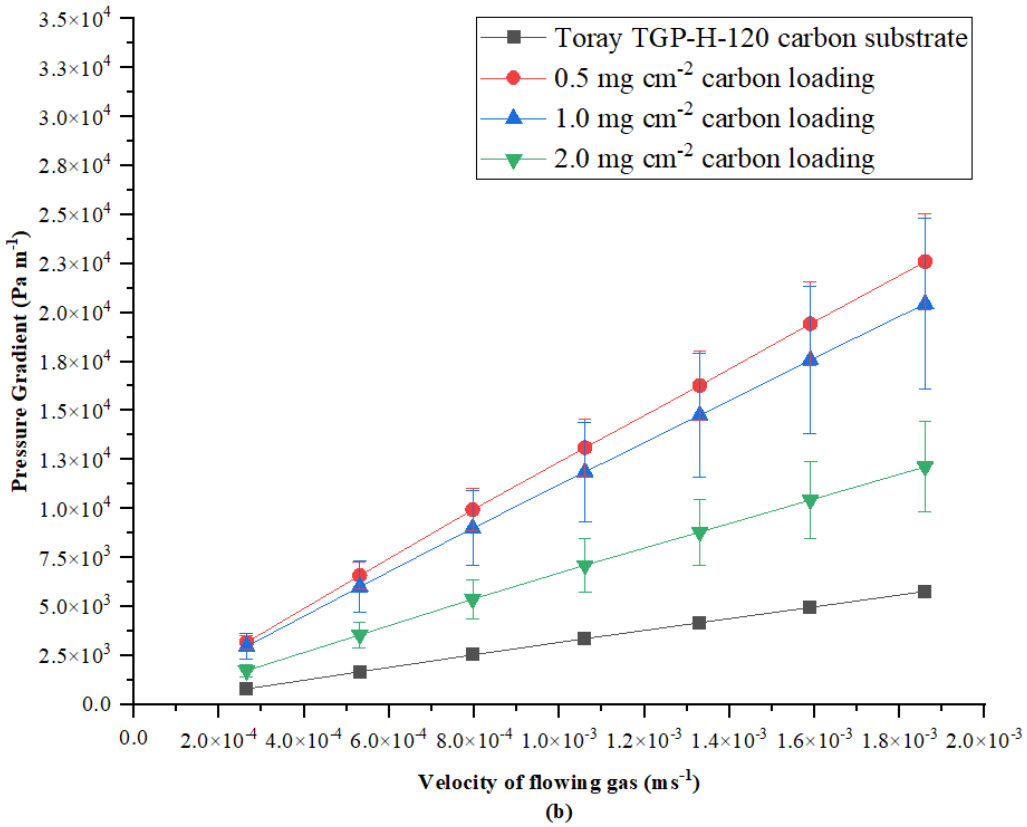
Toray TGP-H-120 carbon substrate
0.5 mg cm-2 carbon loading
1.0 mg cm-2 carbon loading
2.0 mg cm-2 carbon loading
Pressure Gradient (Pa m-1)
Velocity of flowing gas (ms-1)
3.5×10^4
3.3×10^4
3.0×10^4
2.8×10^4
2.5×10^4
2.3×10^4
2.0×10^4
1.8×10^4
1.5×10^4
1.3×10^4
1.0×10^4
7.5×10^3
5.0×10^3
2.5×10^3
0.0
0.0
2.0×10^-4
4.0×10^-4
6.0×10^-4
8.0×10^-4
1.0×10^-3
1.2×10^-3
1.4×10^-3
1.6×10^-3
1.8×10^-3
2.0×10^-3

(b)

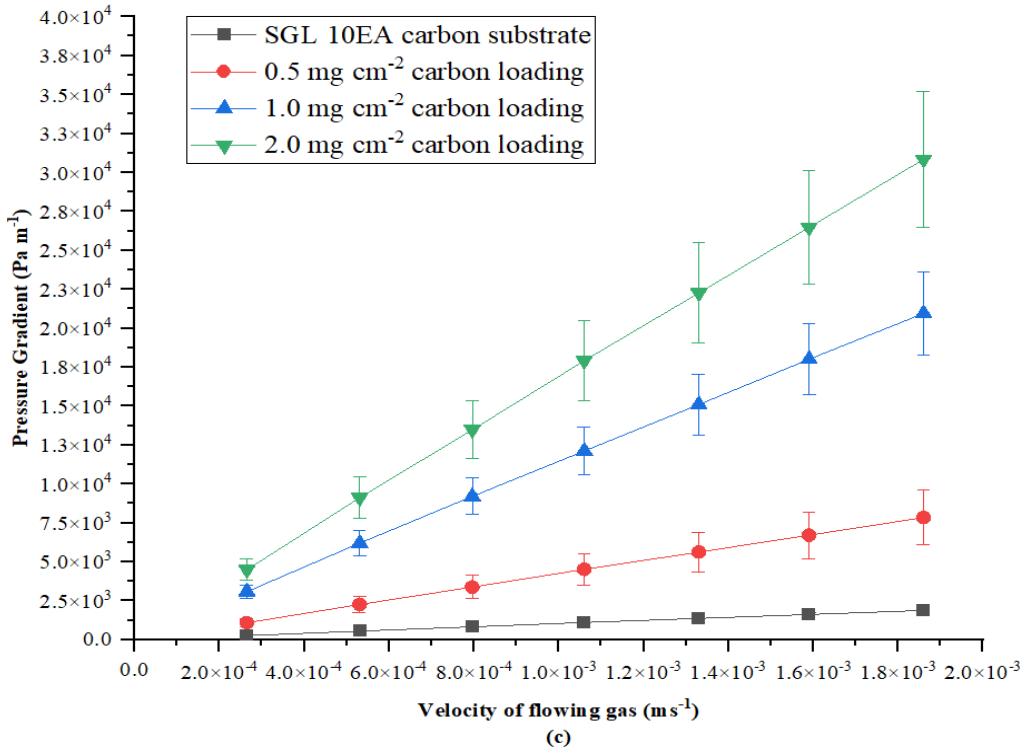
SGL 10EA carbon substrate
0.5 mg cm-2 carbon loading
1.0 mg cm-2 carbon loading
2.0 mg cm-2 carbon loading
Pressure Gradient (Pa m-1)
Velocity of flowing gas (ms-1)
4.0×10^4
3.8×10^4
3.5×10^4
3.3×10^4
3.0×10^4
2.8×10^4
2.5×10^4
2.3×10^4
2.0×10^4
1.8×10^4
1.5×10^4
1.3×10^4
1.0×10^4
7.5×10^3
5.0×10^3
2.5×10^3
0.0
0.0
2.0×10^-4
4.0×10^-4
6.0×10^-4
8.0×10^-4
1.0×10^-3
1.2×10^-3
1.4×10^-3
1.6×10^-3
1.8×10^-3
2.0×10^-3

(c)

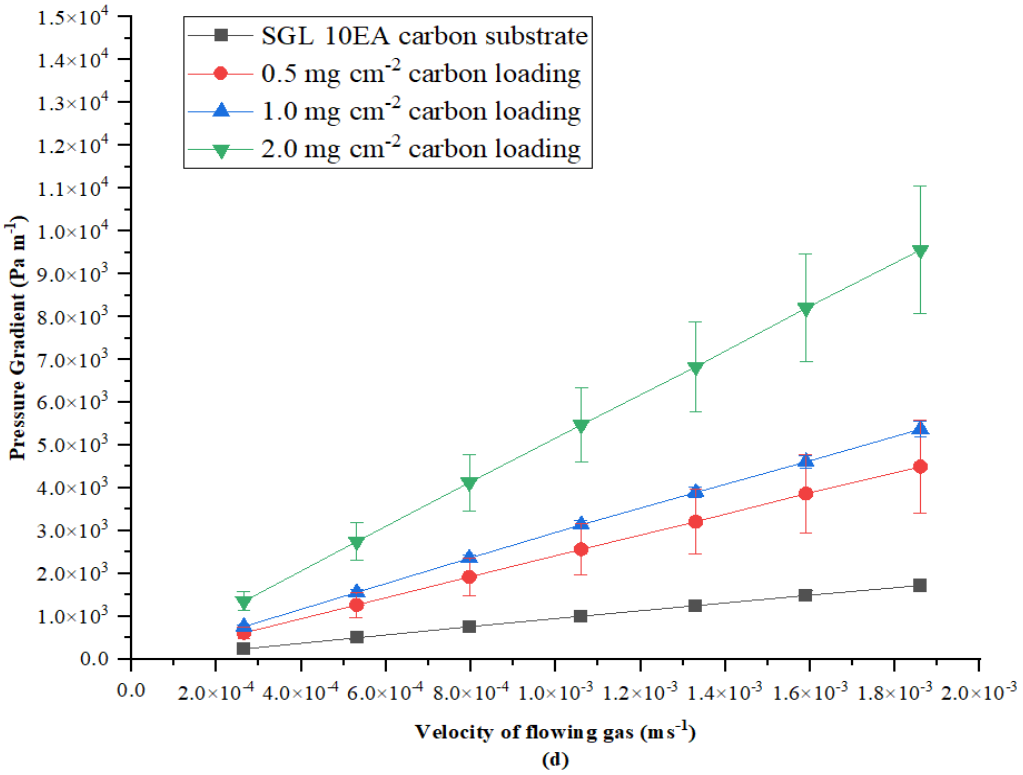

265

266 ***Figure 4. Experimental data for the pressure gradient as a function of fluid velocity for (a-b) Toray-TGP-H 120***
267 ***and (c-d) SGL 10EA coated with Vulcan XC-72R (a, c) and Ketjenblack EC-300J (b, d).***

268 Notably, the pressure gradient increases with the increase in carbon loading for a given velocity
269 in the majority of cases. This trend was seen for both non-woven straight fibre carbon papers
270 (Toray TGP-H-120, Toray TGP-H-90 and SGL 35BA), as well as for felt/spaghetti-like carbon
271 fibre papers (SGL 10CA and SGL 10EA) composed of an MPL using Vulcan XC-72R. The
272 results for SGL 10CA and SGL 10EA are consistent with those reported by Orogbemi et al. in
273 [1], [19] for substrates coated with both Vulcan XC-72R and Ketjenblack EC-300J such that
274 the pressure gradient increases with increasing carbon loading independent of the carbon
275 powder type. This was due to the increase in thickness of the substrates with increased carbon
276 loading. ***Figure 4 (b)***, however, showed an opposite effect with increasing carbon loading, that
277 is, the pressure gradient for a given velocity was the highest at a carbon loading of 0.5 mg cm^{-2}
278 when compared to 2.0 mg cm^{-2} when coated with Ketjenblack EC-300J. This was due to the
279 increase in the size of the cracks on the MPL surface as the carbon loading was increased as

shown in the subsequent section. The through-plane gas permeability of the GDMs is compared in the subsequent section with regard to carbon type and carbon loading (effectively, the thickness of the MPL).

3.2.1 Effect of carbon loading and carbon black type in the microporous layer.

The previous section has demonstrated the significant effect of the increase in carbon loadings in the MPL with the different types of carbon blacks. This varies from what has been reported by Orogbemi et al. [1], [19] and the authors believe these variations were the result of the type of substrate used in combination with the type of carbon black in the MPL. ***Figure 5*** shows the trends in the through-plane gas permeability of the substrates used as a function of carbon loading for the two carbon black types used. The through-plane gas permeability values for the samples shown in Figure 5 can be found in Table A1 of the supplementary material.

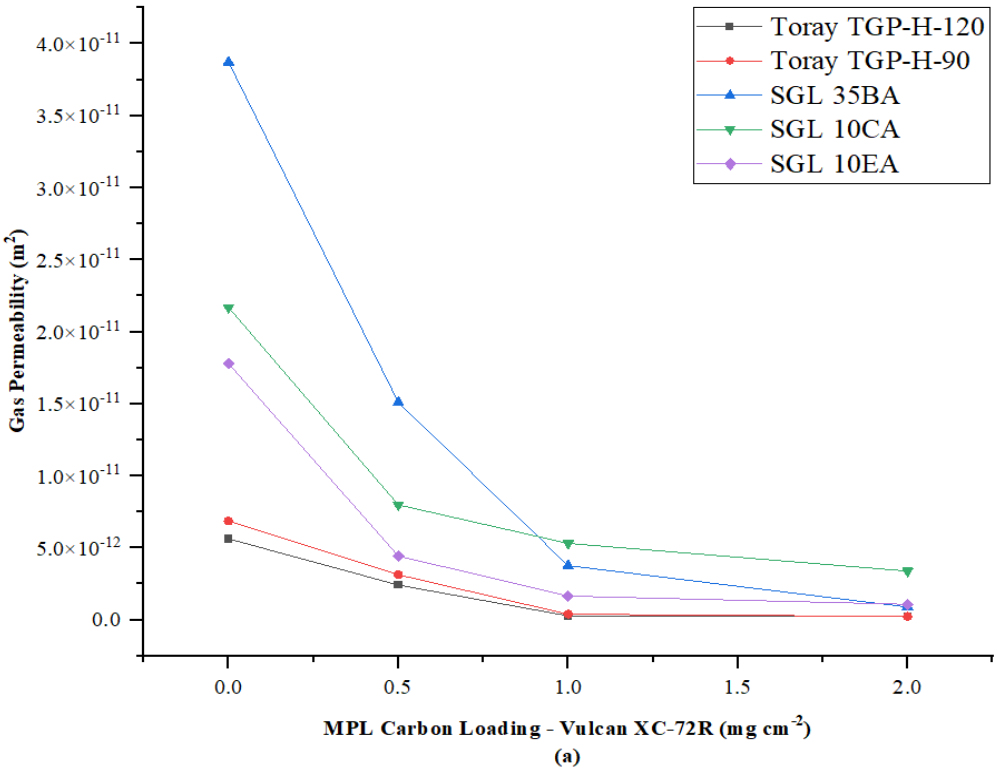

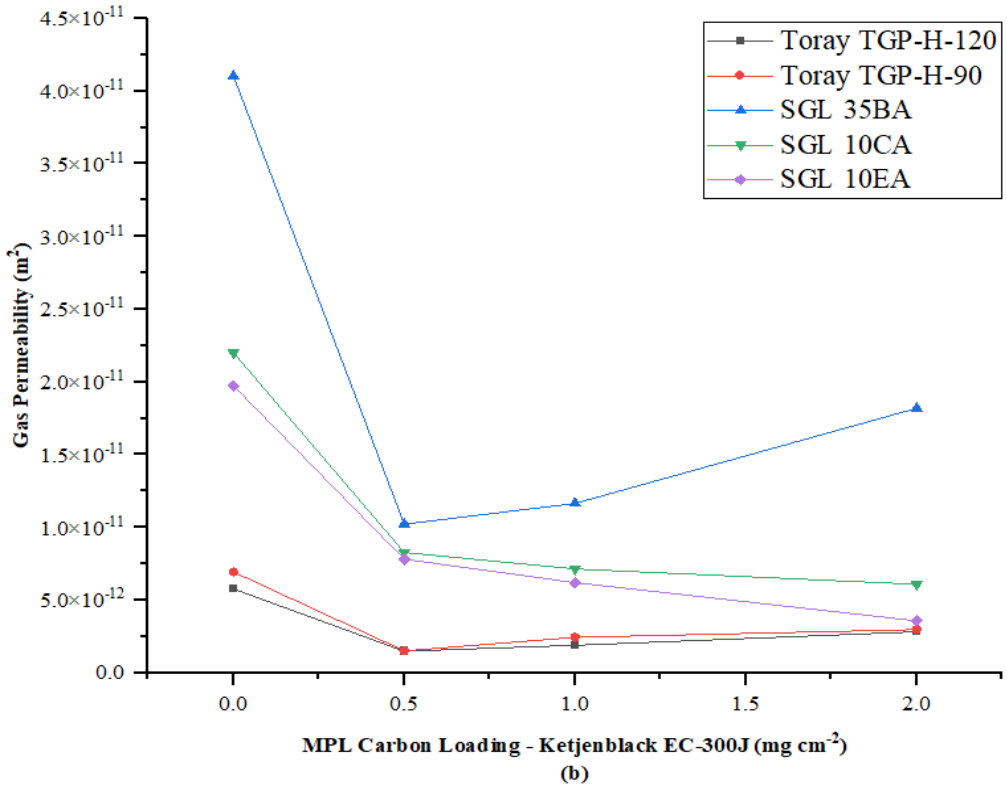

Figure 5. Through-plane gas permeability of GDM for various substrates coated with (a) Vulcan XC-72R and (b) Ketjenblack EC-300J.

For the majority of cases, the increase in carbon loading, after 1 mg cm^{-2}, results in a decrease in the through-plane permeability. The permeability of samples on which the Ketjenblack EC-300J were coated onto, particularly the non-woven straight fibre carbon papers, show an opposite trend, that is, 0.5 mg cm^{-2} carbon loading has the lowest through-plane gas permeability. ***Figure 6*** and ***Figure 7*** show the SEM images of each carbon loading for samples coated with Vulcan XC-72R and Ketjenblack EC-300J for Toray TGP-H-90 and SGL 10EA respectively. The surface morphology of the GDMs using Toray TGP-H-120 and SGL 35BA were similar to those of Toray TGP-H-90 shown in Figure 6 and the GDMs using SGL 10CA were similar that of SGL 10EA shown in Figure 7 for the carbon loadings and carbon powder type.

Figure 6 (a-c) and ***Figure 7 (a-c)***, that is the GDLs coated with Vulcan XC-72R, showed a reduction in the pores with an increase in carbon loading which reflected the decrease in

through-plane permeability with increased carbon loadings. ***Figure 7 (d-f)*** also showed a reduction of pore space in the felt/'spaghetti' structured SGL 10EA with an increase in carbon loading. As such the through-plane gas permeability of GDMs utilising felt/'spaghetti' GDLs was reduced with increasing carbon loading regardless of the carbon powder type. The reductions in the through-plane permeability were at least one order of magnitude lower and in some cases, two orders for carbon loadings between 1.0 mg cm^{-2} and 2.0 mg cm^{-2}. This is in agreement with the results reported in [1], [19].

Figure 6 (d-f) distinctly showed that at a low carbon loading of 0.5 mg cm^{-2}, the pores in the structure are almost completely covered. This justifies the opposite trend shown for GDMs using non-woven straight fibre carbon papers coated with Ketjenblack EC-300J such that at a low carbon loading, the through-plane gas permeability is the lowest. The cracks on the surface increased in size with an increase in carbon loading which is reflected by the increase in through-plane permeability with increased carbon loading for the non-woven straight fibre carbon papers. It is interesting, however, that the surface morphology from Figure 7(e) and 7(f) showed large cracks similar to 6(e) and 6(f) even though the trend in gas permeability increased with carbon loading for the GDMs using non-woven straight fibre GDLs and decreased with carbon loading for the GDMs using felt/'spaghetti' GDLs. El-Kharouf et al. [49] reported porosity values of 67.2%, 61.8% and 70.5% for Toray TGP-H-90, Toray TGP-H-120 and SGL 35BA whilst Gostick et al. [58] reported porosity values for the SGL 10 series to be 84% for SGL 10DA and 86% for SGL 10CA. Since the felt/'spaghetti' type papers, have higher porosities, this may be an indication that even the high surface area powders are able to penetrate the pore space of the felt/'spaghetti' fibre GDLs as the carbon loading is increased resulting in the decrease permeability compared to the opposite effect shown for the non-woven straight fibre papers.

Another interesting observation from Figure 6 (e,f) and 7 (e,f) are the large cracks which develop with the use of the high surface area carbon powder (Ketjenblack EC-300J) regardless of the GDL substrate type at 1.0 and 2.0 mg cm^{-2} carbon loadings. Cracks may be beneficial in the role of water management whereby the cracks provide a preferential pathway for the removal of water from the CL to the GDL [59]; however, some have argued that cracks decrease cell performance by degradation of the mechanical structure of MPL [60] or was influenced by the size of the flow channel in conjunction with these cracks [61] whereas [62] showed that influence of cracks are play a minimal role in cell performance since the majority of water is removed from the CL in vapour form. The surface morphology of the GDMs investigated here would be studied in greater detail in future works to determine their influence on cell performance.

As such, the combination of the various base substrate and type of carbon black played an important role in the resulting trends in through-plane gas permeability of the GDM. Furthermore, the final structure was significantly affected by the properties of the carbon powder type used in combination with the base structure of the GDL. The resulting increase in through-plane permeability for the GDMs which used a combination of non-woven straight fibre carbon papers and Ketjenblack EC-300J was primarily due to the high surface area of the Ketjenblack EC-300J as compared to the Vulcan XC-72R. High surface area carbon powders form large cracks and thicker layers compared to low surface area carbon powders which form smoother surfaces with a dense, thin layer with less cracks [63]. ***Figure 6*** and ***Figure 7*** corroborate this fact.

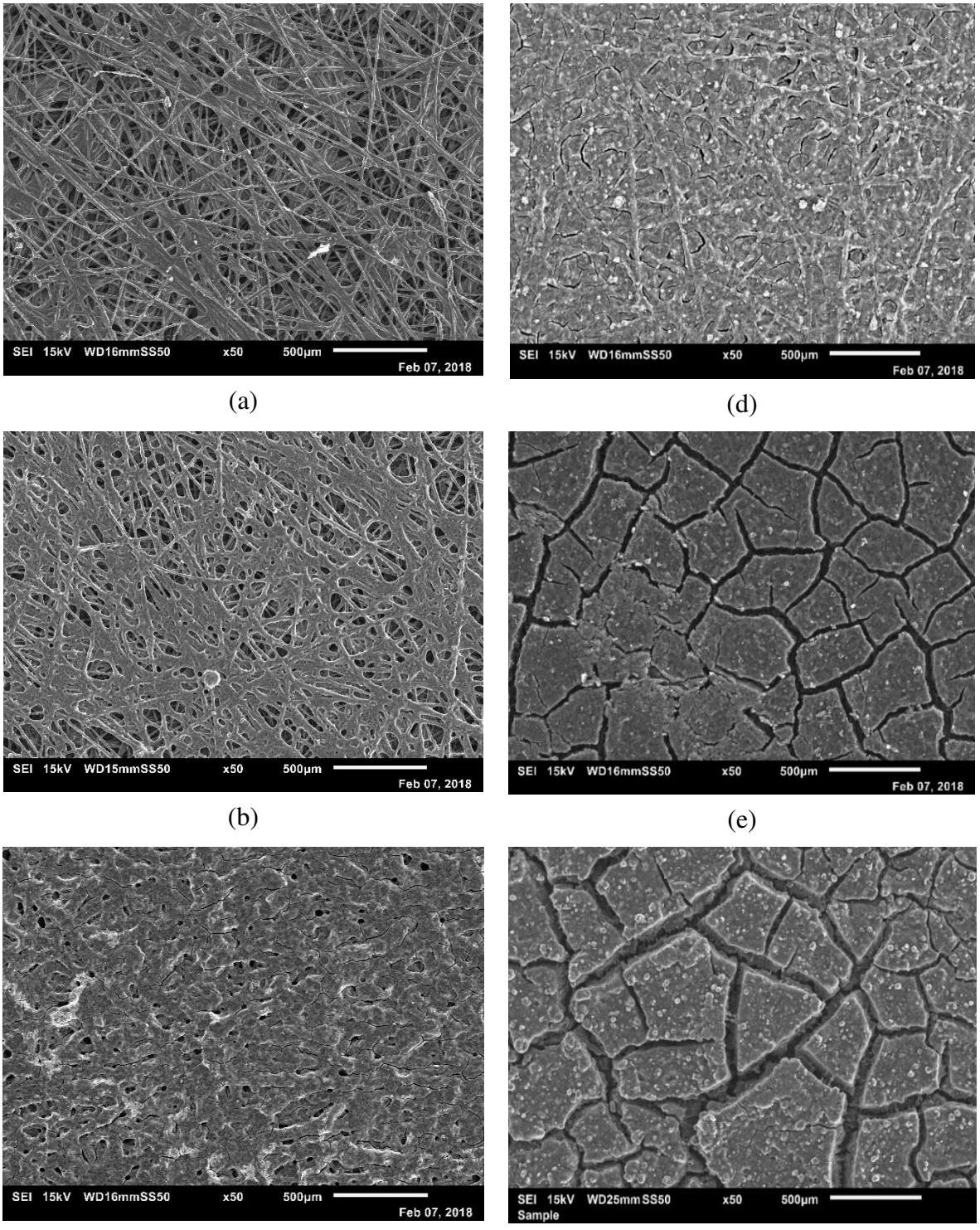

Figure 6. SEM micrographs of Toray TGP-H-90 coated with Vulcan XC-72R (left) and Ketjenblack EC-300J (right) for (a,d) 0.5 mg cm^{-2}, (b,e) 1.0 mg cm^{-2} and (c,f) 2.0 mg cm^{-2}.

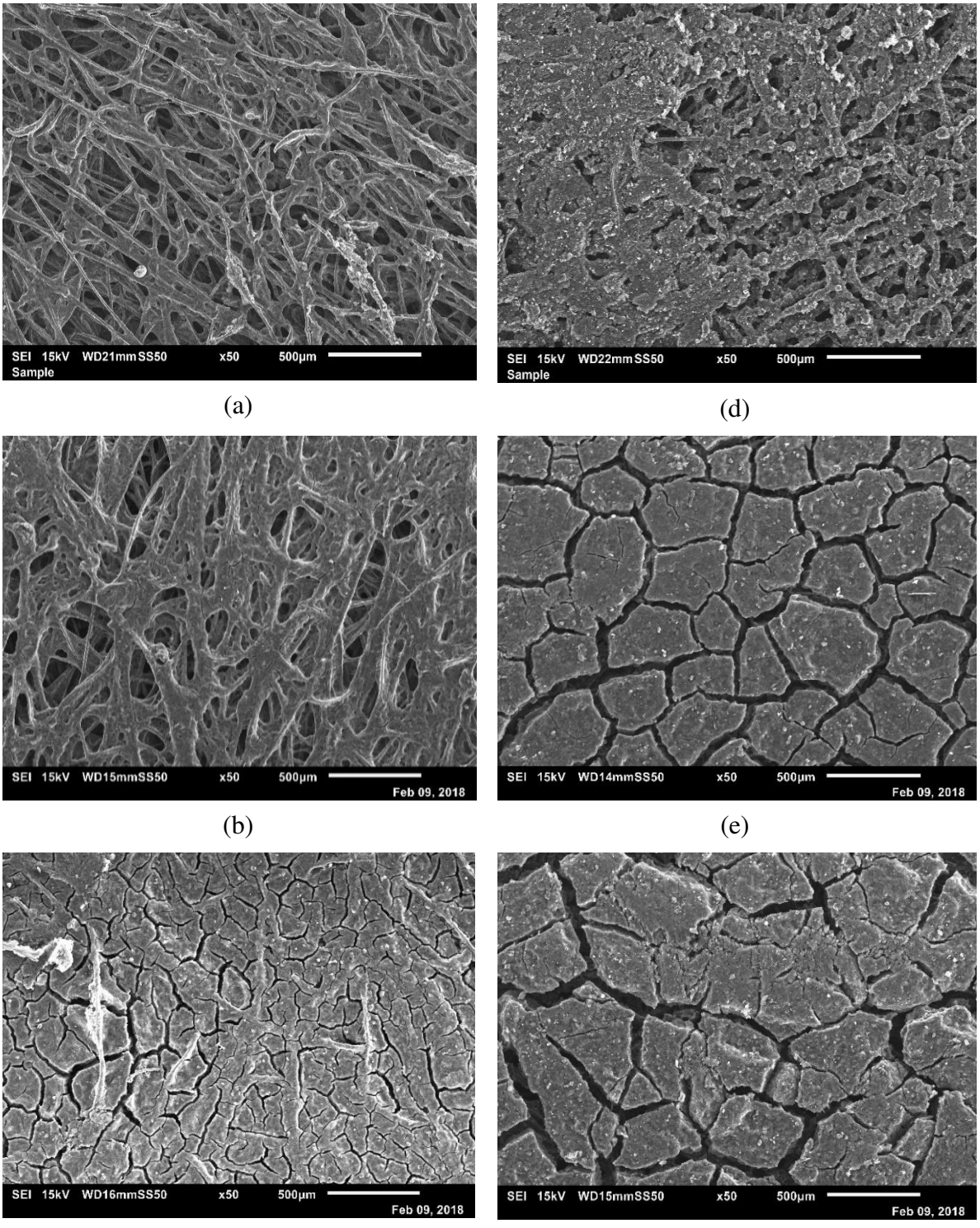

Figure 7. SEM micrographs of SGL 10EA coated with Vulcan XC-72R (left) and Ketjenblack EC-300J (right) for (a,d) 0.5 mg cm^{-2}, (b,e) 1.0 mg cm^{-2} and (c,f) 2.0 mg cm^{-2}.

As stated previously, the increase in carbon loadings increases the thickness of the visible thickness of the MPL. ***Figure 8*** illustrates the increase in thickness with the increase in carbon

loading for the various substrates and carbon black types with the error bars representing the 95% confidence intervals.

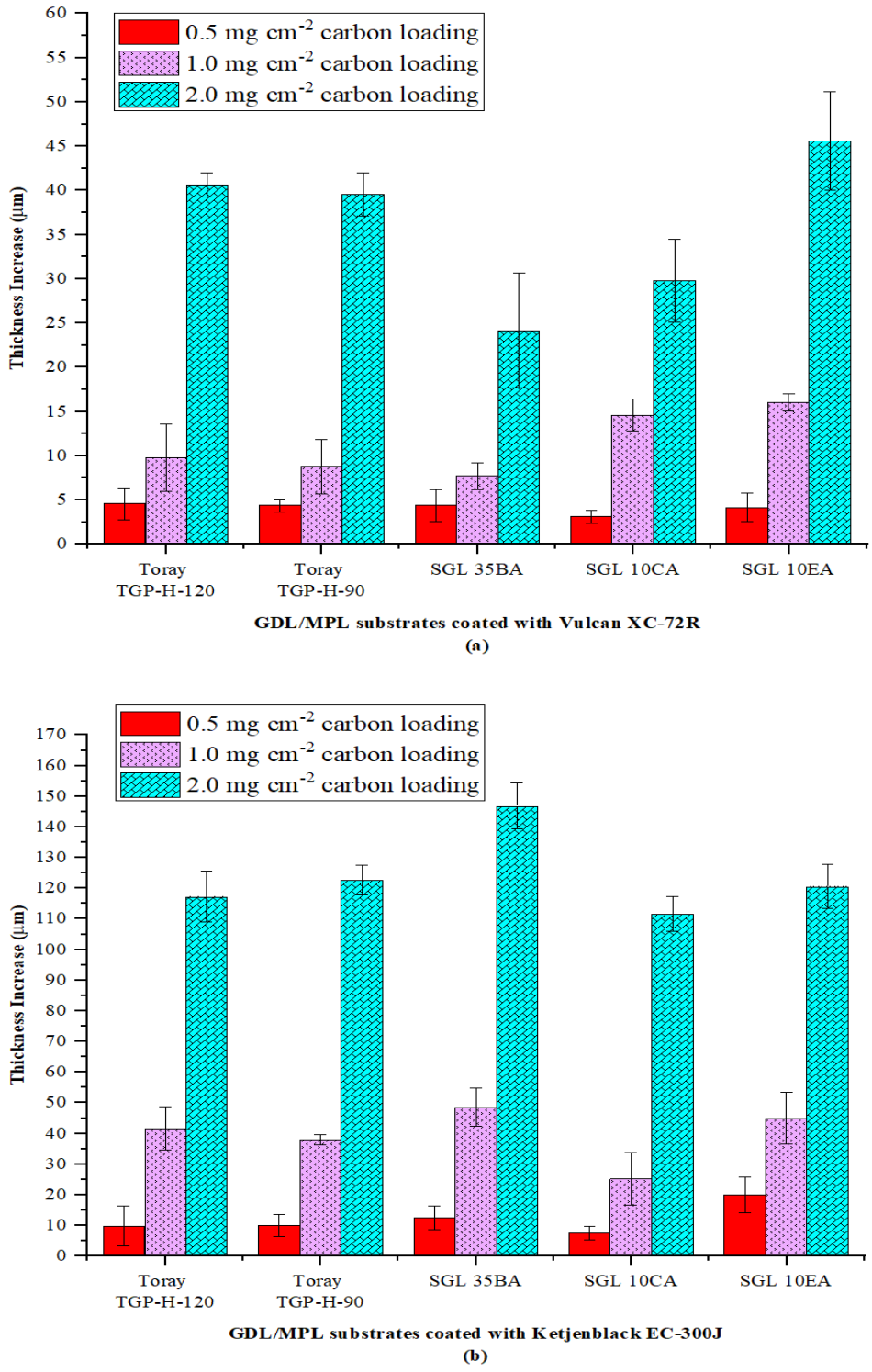

Figure 8. GDL thickness increase for each carbon loading for the various substrates used and coated with the two types of carbon blacks (a) Vulcan XC-72R and (b) Ketjenblack EC-300J.

Figure 8 clearly identifies the significant increase in thickness for the GDLs coated with Ketjenblack EC-300J as opposed to Vulcan XC-72R. As indicated in [1], [19], [26], [57] these variations in thickness were the result of MPL dispersion and penetration into the GDL substrates. ***Figure 9*** shows typical SEM cross sectional images of SGL 10CA for both carbon powders at a 1.0 mg cm^{-2} carbon loading. It is clear, that there is substantial penetration into the GDL structure. The MPL thickness varies considerably, as shown in Figure 9, due to the variations in the penetration into the GDL substrate which is non-uniform. On comparison of Figure 8 and 9, it is clear that the MPL thickness is severely underestimated as suggested in [1], [19] with the penetration of the high surface area carbon powder (Ketjenblack EC-300J) into the GDL substrate being less than that of the low surface area carbon powder (Vulcan XC-72R).

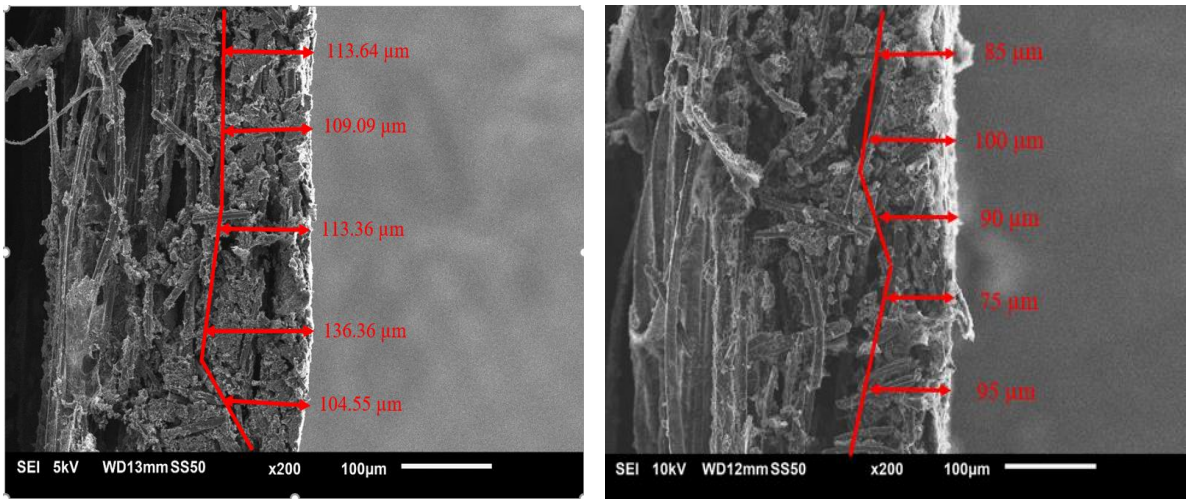

(a) (b)

Figure 9. SEM cross-sectional images of SGL 10CA coated with (a) Vulcan XC-72R and (b) Ketjenblack EC-300J for 1.0 mg cm^{-2} carbon loading respectively.

Furthermore, such variations in the thickness indicate that the properties of the carbon black affect the properties of the MPL in terms of porosity, pore size distribution and surface morphology [15], [49]. Clearly, in all the cases, there is an increase in thickness with an increase in carbon loading and this result is independent of the type of carbon powder used.

This result agrees with the literature found in [1], [19], [64]. El-Kharouf et al. [49] indicated Toray TGP-H-120 and Toray TGP-H-90 share similar properties such as porosity and tortuosity. SGL 35BA was reported to have a slightly higher porosity; however, the tortuosity when compared to that of the Toray carbon papers was found to be far less which would indicate a lower increase in thickness when coated with Vulcan XC-72R as shown in ***Figure 8 (a)***. ***Figure 8 (b)*** showed an increase in thickness for SGL 35BA when compared with that of Toray TGP-H-90 and Toray TGP-H-120 for substrates coated with Ketjenblack EC-300J. This is rather unexpected as the porosity of SGL 35BA is higher and the tortuosity is lower than the Toray carbon papers; this may have been due to fabrication uncertainties as indicated in Section 3.1.

For the felt/'spaghetti' type carbon papers, there is a noticeable increase in thickness with increasing carbon loadings and PTFE in the GDL, as shown in ***Figure 8***. This is understandable since SGL 10EA has a higher PTFE loading (30%) compared with SGL 10CA (10% PTFE loading). The reduced porosity of SGL 10EA would indicate that a smaller amount of carbon ink would be able to penetrate the sample; as such, the visible MPL thickness was higher than that of SGL 10CA.

In the majority of cases, the substrates coated with Ketjenblack EC-300J had a higher through-plane gas permeability when compared to those coated with Vulcan XC-72R due to the large crack formations with increasing carbon loading. The permeability of the non-woven straight carbon fibre substrates at 0.5 mg cm^{-2} had a higher permeability when coated with Vulcan XC-72R as compared to Ketjenblack EC-300J. As the carbon loading was increased, however, the substrates formed a dense, smooth structure resulting in a lower permeability which is in agreement with [63].

3.2.2 Comparison of similar structured GDLs

A comparison of the percentage reduction in gas permeability from the original GDL substrate as a function of carbon black type and carbon loading would be beneficial to compare similar like structures. ***Figure 10*** shows the percentage reduction of through-plane gas permeability from the original sample after coating with each type of carbon black used in this work.

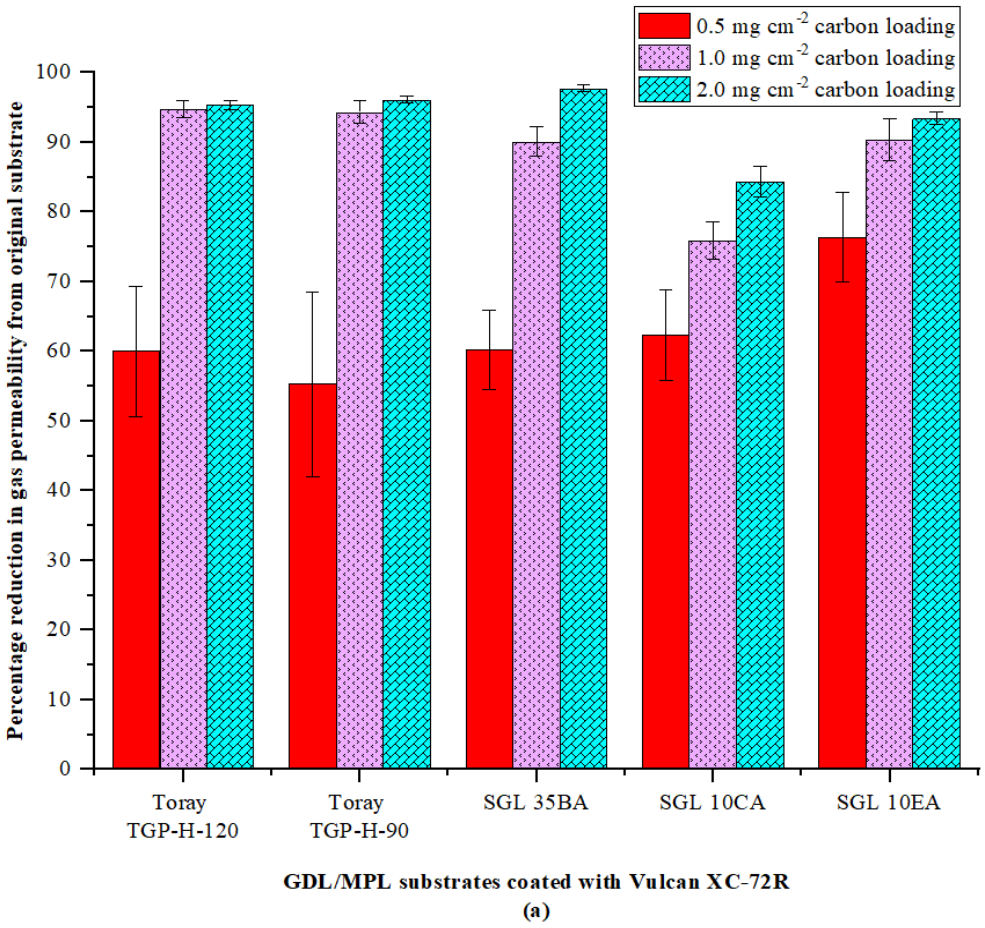

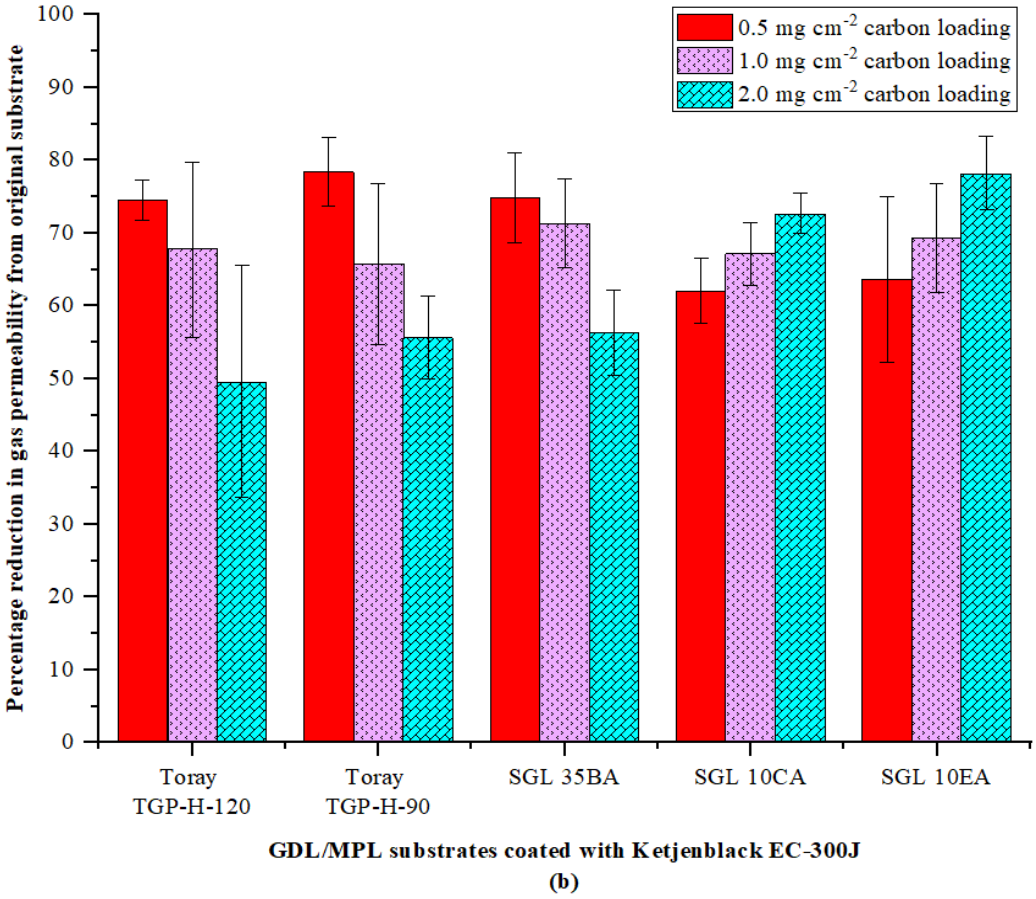

Figure 10. Percentage Reduction in gas permeability from the original substrate for different carbon loadings coated with (a) Vulcan XC-72R and (b) Ketjenblack EC-300J.

The percentage reduction in gas permeability for the non-woven straight fibre carbon papers shows similar reductions for each carbon loading and for each carbon type used. It should be noted that the percentage reduction decreases for the non-woven straight fibre carbon papers with increasing carbon loading which reflects an increase in gas permeability with increasing loading for a high surface area carbon powder (Ketjenblack EC-300J). The felt/'spaghetti' type structures showed a clear distinction in the percentage reduction of gas permeability. This was attributed to the increased PTFE, which resulted in increased thickness due to the lower porosity (blocking of the pores with the increase in carbon loading) as shown in the SEM micrographs in ***Figure 7*** and illustrated in ***Figure 8*** and ***Figure 10***. ***Figure 10 (a) and (b)*** shows that, for SGL 10CA and SGL 10EA coated with Vulcan XC-72R, there is a noticeable difference in the percentage reduction caused by the level of PTFE increase in the GDL

substrates when compared with the relatively small reductions when coated with Ketjenblack EC-300J as the carbon loading was increased. This would imply that the reduction in through-plane gas permeability of the GDM varies depending on the type of carbon black and substrate used; however, depending on the type of carbon black, the level of PTFE in the GDL may either have a huge impact or only slight reduction with an increase in carbon loading.

4. Conclusions

The through-plane gas permeability of different structured GDLs (non-woven straight and felt/'spaghetti') which form the GDM was investigated for MPLs containing two carbon powder types (Vulcan XC-72R and Ketjenblack EC-300J) for various carbon loadings (0.5, 1.0 and 2.0 mg cm^{-2}). The MPL composition of 80 wt. % carbon powder and 20 wt. % PTFE was held constant for all investigations. The impact of increased PTFE loading in the GDL on the through-plane gas permeability and thickness of the GDM was also explored. SEM images were used investigate the surface morphology of the MPL with different carbon loading and types. The main conclusions are as follows:

- GDM through-plane permeability does not necessarily decrease with increased carbon loading. The type of carbon powder and loading used in conjunction with the type of GDL substrate was shown to influence the GDM through-plane permeability. Carbon powders with a high surface area (Ketjenblack EC-300J) showed the greatest reduction in permeability from the original substrate by ~80% for low carbon loadings when coated onto non-woven straight carbon fibre papers with this reduction being as low as ~50% for higher loadings. Non-woven straight fibre carbon papers coated with a low surface area (Vulcan XC-72R) carbon powder showed the greatest reduction in permeability from the original substrate by ~95% for high carbon loadings with this reduction being as low as ~55% for low carbon loadings.

- Surface morphology of the MPLs composed of a carbon powder with a low surface area (Vulcan XC-72R) showed smoother surfaces with smaller crack formation when compared to MPLs composed of a high surface area carbon powder (Ketjenblack EC-300J) which showed significantly larger cracks. Furthermore, the combination of non-woven straight carbon fibre papers with a high surface area carbon powder (Ketjenblack EC-300J) revealed larger surface crack formations with increased carbon loading when compared to the felt/'spaghetti' type fibre papers which showed incomplete coating of the surface for low carbon loadings with cracks being formed as the carbon loadings was increased; however, the permeability of the GDMs utilising felt/'spaghetti' type fibre papers, decreased with increasing carbon loading independent of the carbon type due to the higher porosity of and greater penetration into the GDL substrate.
- GDLs sharing a similar type structure resulted in similar percentage reductions in through-plane permeability from the original substrate when an MPL was applied to it regardless of carbon type and loading. This indicates that, for some GDL materials, the through-plane gas permeability of the GDM may be predictable for a given carbon loading.
- For a given loading of low surface area Vulcan XC-72R carbon powder, the increase in PTFE loading in the GDL, from 10 to 30%, leads to a decrease in gas permeability of the GDM by ~9-15%. Such effect was almost negligible (~2%) for 0.5 and 1.0 mg cm^{-2} carbon loadings but ~5% for 2.0 mg cm^{-2} when high surface area Ketjenblack EC-300J carbon powder is used.

This paper highlights the crucial importance of the GDL base structure on the properties of the GDM. Future works will investigate the use of a wider range of surface area powders to support the findings concluded in this paper and the impact of MPL preparation methods to further

understand and predict the final GDM properties and structure and how these structures influence the performance of a real fuel cell.

Acknowledgements

The first author gratefully acknowledges the financial support of the Scholarships and Advanced Training Division (SATD) within the Ministry of Education in the Republic of Trinidad and Tobago. The authors would like to thank Dr. Alan Dunbar from G67 SEM laboratory at the University of Sheffield for use of the facilities and the Cabot Corporation, USA for supplying the Vulcan XC-72R which was used in this work. Lastly, the author would like to acknowledge the technical support from Mr. Paul Crosby and Dimitry Govorukhin.

References

[1] O. M. Orogbemi, D. B. Ingham, M. S. Ismail, K. J. Hughes, L. Ma, and M. Pourkashanian, "The effects of the composition of microporous layers on the permeability of gas diffusion layers used in polymer electrolyte fuel cells," *Int. J. Hydrogen Energy*, vol. 41, no. 46, pp. 21345–21351, 2016, doi: 10.1016/j.ijhydene.2016.09.160.

[2] F. S. Nanadegani, E. N. Lay, and B. Sunden, "Effects of an MPL on water and thermal management in a PEMFC," *Int. J. Energy Res.*, vol. 43, no. 1, pp. 274–296, 2019, doi: 10.1002/er.4262.

[3] M. S. Ismail, D. Borman, T. Damjanovic, D. B. Ingham, and M. Pourkashanian, "On the through-plane permeability of microporous layer-coated gas diffusion layers used in proton exchange membrane fuel cells," *Int. J. Hydrogen Energy*, vol. 36, no. 16, pp. 10392–10402, 2011, doi: 10.1016/j.ijhydene.2010.09.012.

[4] D. Niblett, A. Mularczyk, V. Niasar, J. Eller, and S. Holmes, "Two-phase flow dynamics

in a gas diffusion layer - gas channel - microporous layer system," *J. Power Sources*, vol. 471, p. 228427, 2020, doi: 10.1016/j.jpowsour.2020.228427.

[5] P. C. Okonkwo and C. Otor, "A review of gas diffusion layer properties and water management in proton exchange membrane fuel cell system," *Int. J. Energy Res.*, vol. 45, no. 3, pp. 3780–3800, 2021, doi: 10.1002/er.6227.

[6] M. Espinoza-Andaluz, R. Reyna, A. Moyón, T. Li, and M. Andersson, "Diffusion parameter correlations for PEFC gas diffusion layers considering the presence of a water-droplet," *Int. J. Hydrogen Energy*, vol. 45, no. 54, pp. 29824–29831, 2020, doi: 10.1016/j.ijhydene.2019.08.144.

[7] G. Karanfil, "Importance and applications of DOE/optimization methods in PEM fuel cells: A review," *Int. J. Energy Res.*, vol. 44, no. 1, pp. 4–25, 2020, doi: 10.1002/er.4815.

[8] J. Liu, S. Shin, and S. Um, "Interfacial transport characteristics between heterogeneous porous composite media for effective mass transfer in fuel cells," *Int. J. Energy Res.*, vol. 43, no. 7, pp. 2990–3005, 2019, doi: 10.1002/er.4500.

[9] A. Ostroverkh *et al.*, "Durable ultra-low-platinum ionomer-free anode catalyst for hydrogen proton exchange membrane fuel cell," *Int. J. Energy Res.*, vol. 44, no. 6, pp. 4641–4651, 2020, doi: 10.1002/er.5245.

[10] L. F. Weng, J. W. Jhuang, M. Bhavanari, K. R. Lee, Y. H. Lai, and C. J. Tseng, "Effects of assembling method and force on the performance of proton-exchange membrane fuel cells with metal foam flow field," *Int. J. Energy Res.*, vol. 44, no. 12, pp. 9707–9713, 2020, doi: 10.1002/er.5611.

[11] Z. Niu, K. Jiao, Y. Wang, Q. Du, and Y. Yin, "Numerical simulation of two-phase cross flow in the gas diffusion layer microstructure of proton exchange membrane fuel cells," *Int. J. Energy Res.*, vol. 42, no. 2, pp. 802–816, 2018, doi: 10.1002/er.3867.

515 [12] S. Waseem, P. H. Maheshwari, S. Abinaya, A. K. Sahu, A. Saini, and S. R. Dhakate,
516 "Effect of matrix content on the performance of carbon paper as an electrode for
517 PEMFC," *Int. J. Energy Res.*, vol. 43, no. 7, pp. 2897–2909, 2019, doi: 10.1002/er.4432.

518 [13] A. El-Kharouf and B. G. Pollet, "Gas Diffusion Media and their Degradation," in *Polymer*
519 *Electrolyte Fuel Cell Degradation*, First Edit., M. M. Mench, E. C. Kumbur, and T. N.
520 Veziroglu, Eds. Academic Press, 2012.

521 [14] C. Lim and C. Y. Wang, "Effects of hydrophobic polymer content in GDL on power
522 performance of a PEM fuel cell," *Electrochim. Acta*, vol. 49, no. 24, pp. 4149–4156,
523 2004, doi: 10.1016/j.electacta.2004.04.009.

524 [15] S. Park, J. W. Lee, and B. N. Popov, "Effect of carbon loading in microporous layer on
525 PEM fuel cell performance," *J. Power Sources*, vol. 163, no. 1 SPEC. ISS., pp. 357–
526 363, 2006, doi: 10.1016/j.jpowsour.2006.09.020.

527 [16] P. Gallo Stampino, L. Omati, C. Cristiani, and G. Dotelli, "Characterisation of
528 nanocarbon-based gas diffusion media by electrochemical impedance spectroscopy,"
529 *Fuel Cells*, vol. 10, no. 2, pp. 270–277, 2010, doi: 10.1002/fuce.200900126.

530 [17] X. Wang, H. Zhang, J. Zhang, H. Xu, X. Zhu, J. Chen and B. Yi, "A bi-functional micro-
531 porous layer with composite carbon black for PEM fuel cells," *J. Power Sources*, vol.
532 162, no. 1, pp. 474–479, 2006, doi: 10.1016/j.jpowsour.2006.06.064.

533 [18] E. Antolini, R. . Passos, and E. . Ticianelli, "Effects of the carbon powder characteristics
534 in the cathode gas diffusion layer on the performance of polymer electrolyte fuel cells,"
535 *J. Power Sources*, vol. 109, no. 2, pp. 477–482, 2002, doi: 10.1016/S0378-
536 7753(02)00112-X.

537 [19] O. M. Orogbemi, D. B. Ingham, M. S. Ismail, K. J. Hughes, L. Ma, and M.
538 Pourkashanian, "Through-plane gas permeability of gas diffusion layers and

539 microporous layer: Effects of carbon loading and sintering," *J. Energy Inst.*, vol. 91, no.
540 2, pp. 270–278, 2018, doi: 10.1016/j.joei.2016.11.008.

541 [20] M. Han, S. H. Chan, and S. P. Jiang, "Development of carbon-filled gas diffusion layer
542 for polymer electrolyte fuel cells," *J. Power Sources*, vol. 159, no. 2, pp. 1005–1014,
543 2006, doi: 10.1016/j.jpowsour.2005.12.003.

544 [21] S. B. Park, S. Kim, Y. Il Park, and M. H. Oh, "Fabrication of GDL microporous layer
545 using PVDF for PEMFCs," *J. Phys. Conf. Ser.*, vol. 165, 2009, doi: 10.1088/1742-
546 6596/165/1/012046.

547 [22] A. Ong, A. Bottino, G. Capannelli, and A. Comite, "Effect of preparative parameters on
548 the characteristic of poly(vinylidene fluoride)-based microporous layer for proton
549 exchange membrane fuel cells," *J. Power Sources*, vol. 183, no. 1, pp. 62–68, 2008, doi:
550 10.1016/j.jpowsour.2008.04.064.

551 [23] S. B. Park and Y. il Park, "Fabrication of gas diffusion layer (GDL) containing
552 microporous layer using flourinated ethylene prophylene (FEP) for proton exchange
553 membrane fuel cell (PEMFC)," *Int. J. Precis. Eng. Manuf.*, vol. 13, no. 7, pp. 1145–
554 1151, 2012, doi: 10.1007/s12541-012-0152-x.

555 [24] H. Gharibi, M. Javaheri, and R. A. Mirzaie, "The synergy between multi-wall carbon
556 nanotubes and Vulcan XC72R in microporous layers," *Int. J. Hydrogen Energy*, vol. 35,
557 no. 17, pp. 9241–9251, 2010, doi: 10.1016/j.ijhydene.2009.08.092.

558 [25] E. Passalacqua, G. Squadrito, F. Lufrano, A. Patti, and L. Giorgi, "Effects of the diffusion
559 layer characteristics on the performance of polymer electrolyte fuel cell electrodes," *J.*
560 *Appl. Electrochem.*, vol. 31, no. 4, pp. 449–454, 2001, doi: 10.1023/A:1017547112282.

561 [26] L. R. Jordan, A.K. Shukla, T. Behrsing, N.R. Avery, B.C. Muddle, and M. Forsyth,
562 "Diffusion layer parameters influencing optimal fuel cell performance," *J. Power*

563 *Sources*, vol. 86, no. 1–2, pp. 250–254, 2000, doi: 10.1016/S0378-7753(99)00489-9.

564 [27] J. Chen, T. Matsuura, and M. Hori, "Novel gas diffusion layer with water management
565 function for PEMFC," *J. Power Sources*, vol. 131, no. 1–2, pp. 155–161, 2004, doi:
566 10.1016/j.jpowsour.2004.01.007.

567 [28] A. Z. Weber and J. Newman, "Effects of Microporous Layers in Polymer Electrolyte Fuel
568 Cells," *J. Electrochem. Soc.*, vol. 152, no. 4, p. A677, 2005, doi: 10.1149/1.1861194.

569 [29] C. Fan and M. Chang, "Improving proton exchange membrane fuel cell performance with
570 carbon nanotubes as the material of cathode microporous layer," *Int. J. Energy Res.*, vol.
571 40, no. 2, pp. 181-188, 2016, doi: 10.1002/er.3445.

572 [30] M. Mariani, S. Latorrata, P. Gallo Stampino, and G. Dotelli, "Evaluation of Graphene
573 Nanoplatelets as a Microporous Layer Material for PEMFC: Performance and Durability
574 Analysis," *Fuel Cells*, vol. 19, no. 6, pp. 685–694, 2019, doi: 10.1002/fuce.201900110.

575 [31] A. Öztürk, B. Fıçıcılar, İ. Eroğlu, and A. Bayrakçeken Yurtcan, "Facilitation of water
576 management in low Pt loaded PEM fuel cell by creating hydrophobic microporous layer
577 with PTFE, FEP and PDMS polymers: Effect of polymer and carbon amounts," *Int. J.*
578 *Hydrogen Energy*, vol. 42, no. 33, pp. 21226–21249, 2017, doi:
579 10.1016/j.ijhydene.2017.06.202.

580 [32] M. Mariani, S. Latorrata, S. Patrignani, P. Gallo Stampino, and G. Dotelli,
581 "Characterization of novel graphene-based microporous layers for Polymer Electrolyte
582 Membrane Fuel Cells operating under low humidity and high temperature," *Int. J.*
583 *Hydrogen Energy*, vol. 45, no. 11, pp. 7046–7058, 2020, doi:
584 10.1016/j.ijhydene.2019.12.213.

585 [33] L. Chen, R. Lin, S. Tang, D. Zhong, and Z. Hao, "Structural design of gas diffusion layer
586 for proton exchange membrane fuel cell at varying humidification," *J. Power Sources*,

587 vol. 467, no. April, p. 228355, 2020, doi: 10.1016/j.jpowsour.2020.228355.

588 [34] X. Fu, H. Ni, F. Zhang, Y. Yang, X. Shao, Z. Huang, R. Zhang, Q. Liu and S. Hu,
589 "Polypyrrole nanowires as a cathode microporous layer for direct methanol fuel cell to
590 enhance oxygen transport," *Int. J. Energy Res.*, vol. 45, no. 2, pp. 3375–3384, 2021, doi:
591 10.1002/er.5976.

592 [35] A. Tamayol, F. McGregor, and M. Bahrami, "Single phase through-plane permeability
593 of carbon paper gas diffusion layers," *J. Power Sources*, vol. 204, pp. 94–99, 2012, doi:
594 10.1016/j.jpowsour.2011.11.084.

595 [36] M. S. Ismail, T. Damjanovic, K. Hughes, D.B. Ingham, L. Ma, M. Pourkashanian and M.
596 Rosli, "Through-Plane Permeability for Untreated and PTFE-Treated Gas Diffusion
597 Layers in Proton Exchange Membrane Fuel Cells," *J. Fuel Cell Sci. Technol.*, vol. 7, no.
598 5, p. 051016, 2010, doi: 10.1115/1.4000685.

599 [37] M. V Williams, E. Begg, L. Bonville, H. R. Kunz, and J. M. Fenton, "Characterization
600 of gas diffusion layers for PEMFC," *J. Electrochem. Soc.*, vol. 151, no. 8, pp. A1173–
601 A1180, 2004, doi: Doi 10.1149/1.1764779.

602 [38] J. Ihonen, M. Mikkola, and G. Lindbergh, "Flooding of gas diffusion backing in PEFCs:
603 Physical and electrochemical characterization," *J. Electrochem. Soc.*, vol. 151, no. 8, pp.
604 1152–1161, 2004, doi: 10.1149/1.1763138.

605 [39] M. S. Ismail, T. Damjanovic, D. B. Ingham, L. Ma, and M. Pourkashanian, "Effect of
606 polytetrafluoroethylene-treatment and microporous layer-coating on the in-plane
607 permeability of gas diffusion layers used in proton exchange membrane fuel cells," *J.*
608 *Power Sources*, vol. 195, no. 19, pp. 6619–6628, 2010, doi:
609 10.1016/j.jpowsour.2010.04.036.

610 [40] V. Gurau, M. J. Bluemle, E. S. De Castro, Y. M. Tsou, T. A. Zawodzinski, and J. A.

611 Mann, “Characterization of transport properties in gas diffusion layers for proton
612 exchange membrane fuel cells. 2. Absolute permeability,” *J. Power Sources*, vol. 165,
613 no. 2, pp. 793–802, 2007, doi: 10.1016/j.jpowsour.2006.12.068.

614 [41] H. Dohle, R. Jung, N. Kimiaie, J. Mergel, and M. Müller, “Interaction between the
615 diffusion layer and the flow field of polymer electrolyte fuel cells - Experiments and
616 simulation studies,” *J. Power Sources*, vol. 124, no. 2, pp. 371–384, 2003, doi:
617 10.1016/S0378-7753(03)00800-0.

618 [42] D. Bevers, R. Rogers, and M. Von Bradke, “Examination of the influence of PTFE
619 coating on the properties of carbon paper in polymer electrolyte fuel cells,” *J. Power*
620 *Sources*, vol. 63, no. 2, pp. 193–201, 1996, doi: 10.1016/S0378-7753(96)02465-2.

621 [43] G. G. Park, Y. J. Sohn, T. H. Yang, Y. G. Yoon, W. Y. Lee, and C. S. Kim, “Effect of
622 PTFE contents in the gas diffusion media on the performance of PEMFC,” *J. Power*
623 *Sources*, vol. 131, no. 1–2, pp. 182–187, 2004, doi: 10.1016/j.jpowsour.2003.12.037.

624 [44] J. G. Pharoah, “On the permeability of gas diffusion media used in PEM fuel cells,” *J.*
625 *Power Sources*, vol. 144, no. 1, pp. 77–82, 2005, doi: 10.1016/j.jpowsour.2004.11.069.

626 [45] D. Tehlar, R. Flückiger, A. Wokaun, and F. N. Büchi, “Investigation of channel-to-
627 channel cross convection in serpentine flow fields,” *Fuel Cells*, vol. 10, no. 6, pp. 1040–
628 1049, 2010, doi: 10.1002/fuce.201000034.

629 [46] J. P. Feser, A. K. Prasad, and S. G. Advani, “Experimental characterization of in-plane
630 permeability of gas diffusion layers,” *J. Power Sources*, vol. 162, no. 2 SPEC. ISS., pp.
631 1226–1231, 2006, doi: 10.1016/j.jpowsour.2006.07.058.

632 [47] P. Mangal, L. Pant, N. Carrigy, M. Dumontier and V. Zingan, “Experimental study of
633 mass transport in PEMFCs: Through plane permeability and molecular diffusivity in
634 GDLs,” *Electrochim. Acta*, vol. 167, pp. 160–171, 2015, doi:

635 10.1016/j.electacta.2015.03.100.

636 [48] J. T. Gostick, M. W. Fowler, M. D. Pritzker, M. A. Ioannidis, and L. M. Behra, "In-plane
637 and through-plane gas permeability of carbon fiber electrode backing layers," *J. Power*
638 *Sources*, vol. 162, no. 1, pp. 228–238, 2006, doi: 10.1016/j.jpowsour.2006.06.096.

639 [49] A. El-Kharouf, T. J. Mason, D. J. L. Brett, and B. G. Pollet, "Ex-situ characterisation of
640 gas diffusion layers for proton exchange membrane fuel cells," *J. Power Sources*, vol.
641 218, pp. 393–404, 2012, doi: 10.1016/j.jpowsour.2012.06.099.

642 [50] D. Froning, M. Drakselová, A. Tocháčková, R. Kodym, U. Reimer, W. Lehnert and K.
643 Bouzek, "Anisotropic properties of gas transport in non-woven gas diffusion layers of
644 polymer electrolyte fuel cells," *J. Power Sources*, vol. 452, no. February, 2020, doi:
645 10.1016/j.jpowsour.2020.227828

646 [51] M. Mukherjee, C. Bonnet, and F. Lapicque, "Estimation of through-plane and in-plane
647 gas permeability across gas diffusion layers (GDLs): Comparison with equivalent
648 permeability in bipolar plates and relation to fuel cell performance," *Int. J. Hydrogen*
649 *Energy*, vol. 45, no. 24, pp. 13428–13440, 2020, doi: 10.1016/j.ijhydene.2020.03.026.

650 [52] F. Aldakheel, M. S. Ismail, K. J. Hughes, D. B. Ingham, L. Ma, M. Pourkashanian, D.
651 Cumming and R. Smith, "Gas permeability, wettability and morphology of gas diffusion
652 layers before and after performing a realistic ex-situ compression test," *Renew. Energy*,
653 vol. 151, pp. 1082–1091, 2020, doi: 10.1016/j.renene.2019.11.109.

654 [53] N. B. Carrigy, L. M. Pant, S. Mitra, and M. Secanell, "Knudsen Diffusivity and
655 Permeability of PEMFC Microporous Coated Gas Diffusion Layers for Different
656 Polytetrafluoroethylene Loadings," *J. Electrochem. Soc.*, vol. 160, no. 2, pp. F81–F89,
657 2012, doi: 10.1149/2.036302jes.

658 [54] G. Unsworth, L. Dong, and X. Li, "Improved experimental method for measuring gas

659 diffusivity through thin porous media," *AlChe*, vol. 59, no. 4, pp. 1409–1419, 2013.

660 [55] P. H. Maheshwari, R. B. Mathur, and T. L. Dhami, "The influence of the pore size and
661 its distribution in a carbon paper electrode on the performance of a PEM Fuel cell,"
662 *Electrochim. Acta*, vol. 54, no. 2, pp. 655–659, 2008, doi:
663 10.1016/j.electacta.2008.07.029.

664 [56] M. Uchida, Y. Aoyama, N. Eda, and A. Ohta, "Investigation of the Microstructure in the
665 Catalyst Layer and Effects of Both Perfluorosulfonate lonomer and PTFE-Loaded
666 Carbon on the Catalyst Layer of Polymer Electrolyte Fuel Cells," *J. Electrochem. Soc.*,
667 vol. 142, no. 12, pp. 4143–4149, 1995, doi: 10.1149/1.2048477.

668 [57] T. Kitahara, T. Konomi, and H. Nakajima, "Microporous layer coated gas diffusion layers
669 for enhanced performance of polymer electrolyte fuel cells," *J. Power Sources*, vol. 195,
670 no. 8, pp. 2202–2211, 2010, doi: 10.1016/j.jpowsour.2009.10.089.

671 [58] J. T. Gostick, M. A. Ioannidis, M. W. Fowler, and M. D. Pritzker, "Wettability and
672 capillary behavior of fibrous gas diffusion media for polymer electrolyte membrane fuel
673 cells," *J. Power Sources*, vol. 194, no. 1, pp. 433–444, 2009, doi:
674 10.1016/j.jpowsour.2009.04.052.

675 [59] R. Omrani and B. Shabani, "Gas diffusion layer modifications and treatments for
676 improving the performance of proton exchange membrane fuel cells and electrolysers:
677 A review," *Int. J. Hydrogen Energy*, vol. 42, no. 47, pp. 28515–28536, 2017, doi:
678 10.1016/j.ijhydene.2017.09.132.

679 [60] J. H. Chun, D. H. Jo, S. G. Kim, S. H. Park, C. H. Lee, and S. H. Kim, "Improvement of
680 the mechanical durability of micro porous layer in a proton exchange membrane fuel
681 cell by elimination of surface cracks," *Renew. Energy*, vol. 48, pp. 35–41, 2012, doi:
682 10.1016/j.renene.2012.04.011.

683 [61] G. H. Kim, D. Kim, J. Kim, H. Kim, and T. Park, “Impact of cracked gas diffusion layer
684 on performance of polymer electrolyte membrane fuel cells,” *J. Ind. Eng. Chem.*, vol.
685 91, pp. 311–316, 2020, doi: 10.1016/j.jiec.2020.08.014.

686 [62] J. P. Owejan, J. E. Owejan, W. Gu, T. A. Trabold, T. W. Tighe, and M. F. Mathias,
687 “Water Transport Mechanisms in PEMFC Gas Diffusion Layers,” *J. Electrochem. Soc.*,
688 vol. 157, no. 10, p. B1456, 2010, doi: 10.1149/1.3468615.

689 [63] A. Ozden, S. Shahgaldi, J. Zhao, X. Li, and F. Hamdullahpur, “Assessment of graphene
690 as an alternative microporous layer material for proton exchange membrane fuel cells,”
691 *Fuel*, vol. 215, no. November 2017, pp. 726–734, 2018, doi: 10.1016/j.fuel.2017.11.109.

692 [64] M. Prasanna, H. Y. Ha, E. A. Cho, S. A. Hong, and I. H. Oh, “Influence of cathode gas
693 diffusion media on the performance of the PEMFCs,” *J. Power Sources*, vol. 131, no.
694 1–2, pp. 147–154, 2004, doi: 10.1016/j.jpowsour.2004.01.030.

695

696
697

698 **Supplementary Material**

699

700

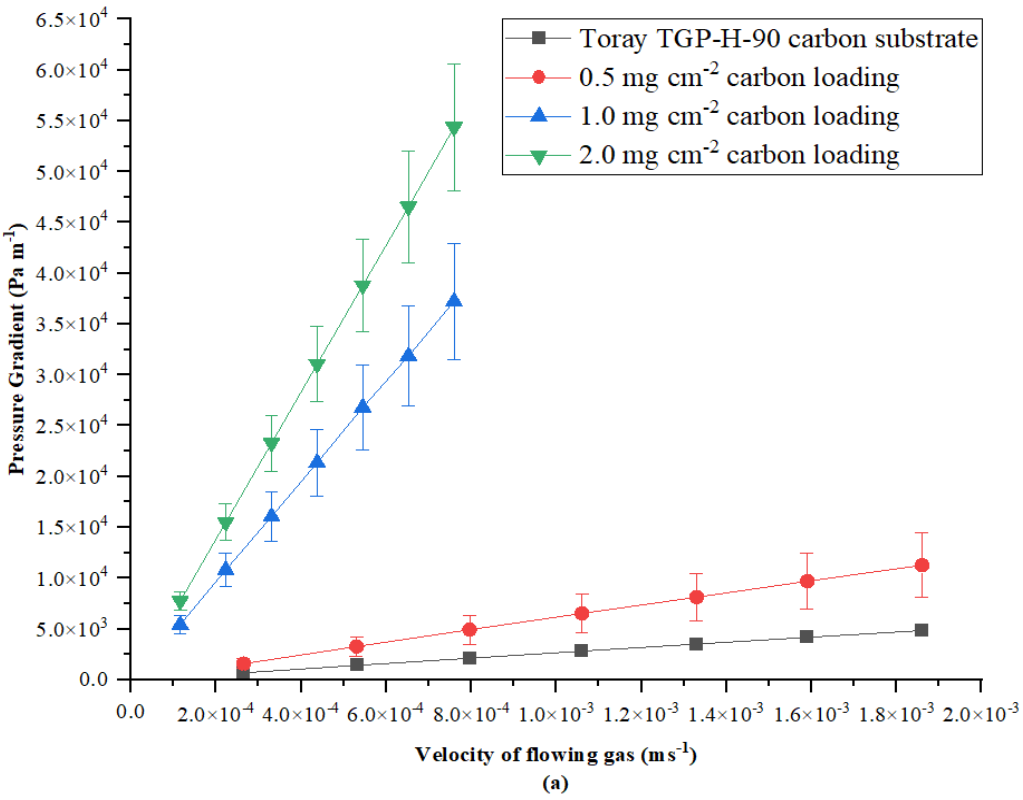

(a)

701

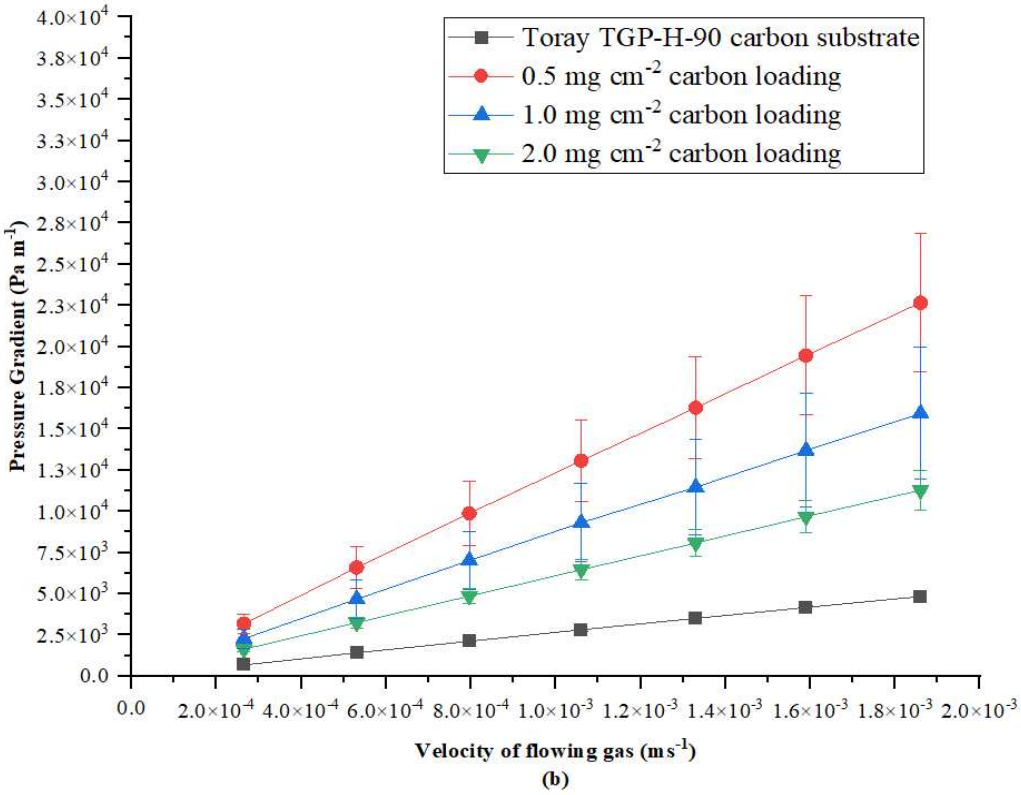
Toray TGP-H-90 carbon substrate
0.5 mg cm-2 carbon loading
1.0 mg cm-2 carbon loading
2.0 mg cm-2 carbon loading
Pressure Gradient (Pa m-1)
Velocity of flowing gas (ms-1)

(b)

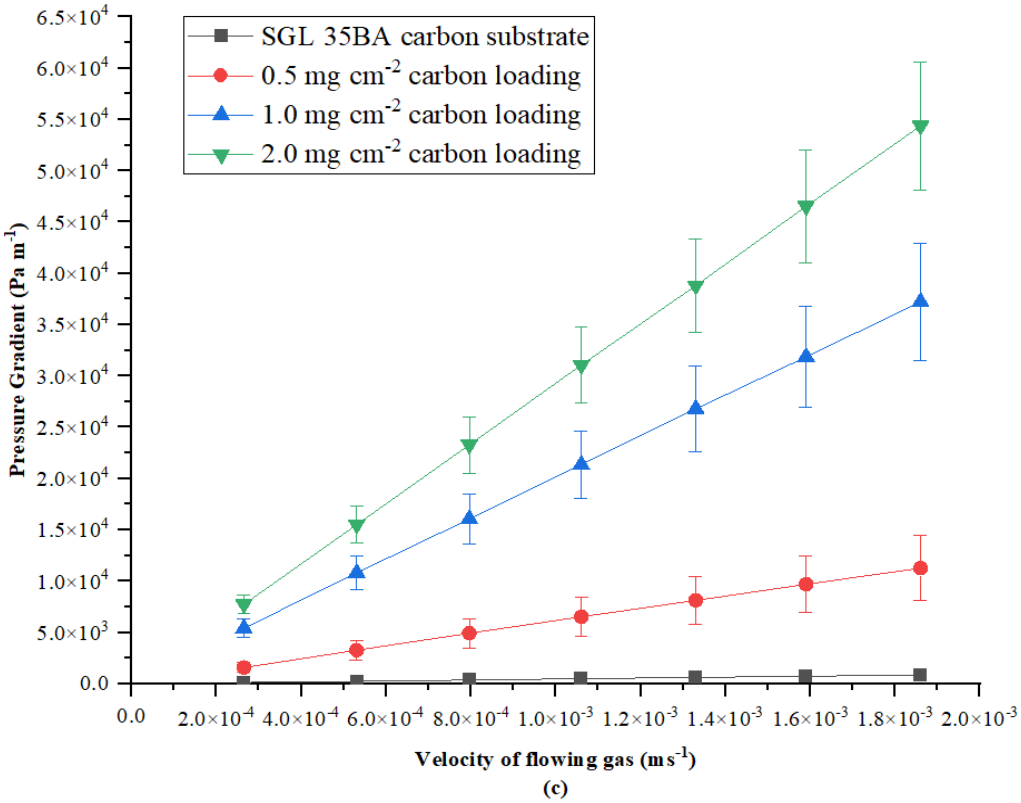
SGL 35BA carbon substrate
0.5 mg cm-2 carbon loading
1.0 mg cm-2 carbon loading
2.0 mg cm-2 carbon loading
Pressure Gradient (Pa m-1)
Velocity of flowing gas (ms-1)

(c)

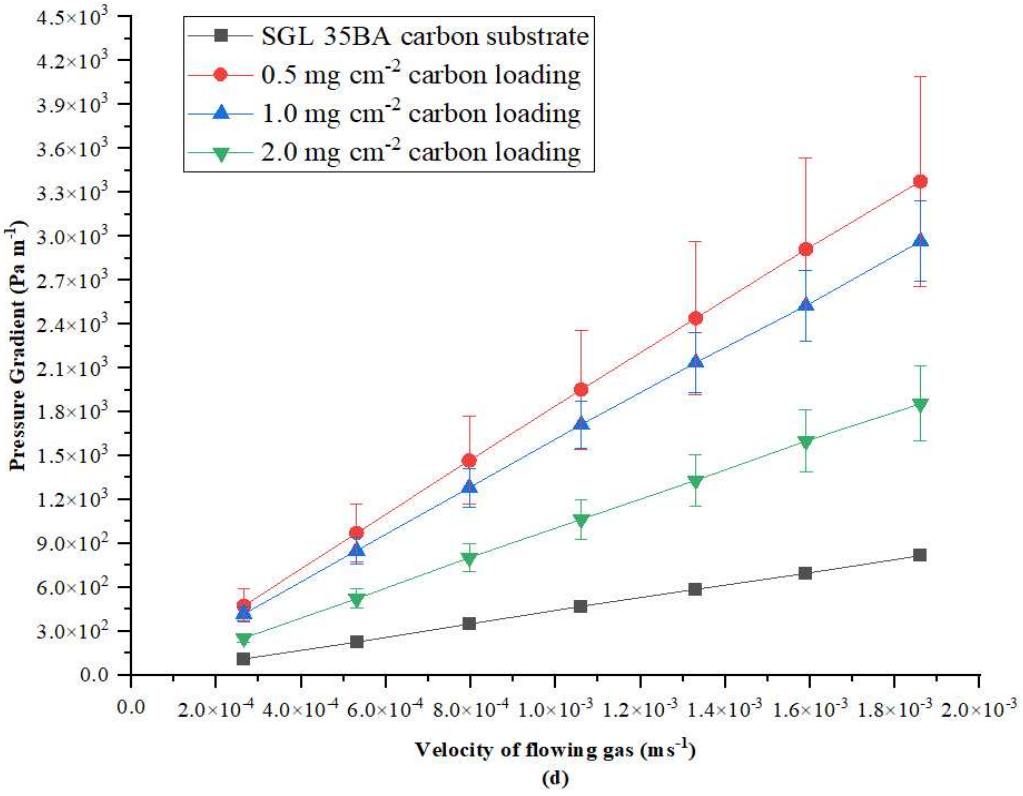
SGL 35BA carbon substrate
0.5 mg cm-2 carbon loading
1.0 mg cm-2 carbon loading
2.0 mg cm-2 carbon loading
Pressure Gradient (Pa m-1)
Velocity of flowing gas (ms-1)
0.0
3.0×10^2
6.0×10^2
9.0×10^2
1.2×10^3
1.5×10^3
1.8×10^3
2.1×10^3
2.4×10^3
2.7×10^3
3.0×10^3
3.3×10^3
3.6×10^3
3.9×10^3
4.2×10^3
4.5×10^3
2.0×10^-4
4.0×10^-4
6.0×10^-4
8.0×10^-4
1.0×10^-3
1.2×10^-3
1.4×10^-3
1.6×10^-3
1.8×10^-3
2.0×10^-3

(d)

704

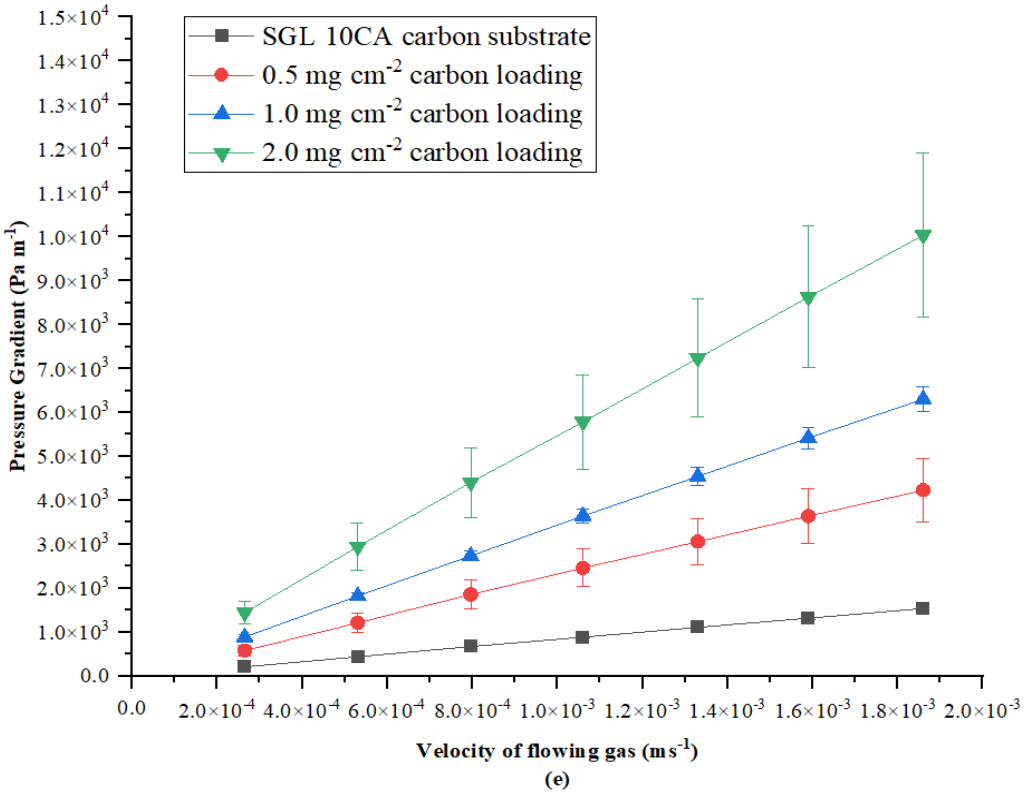
SGL 10CA carbon substrate
0.5 mg cm-2 carbon loading
1.0 mg cm-2 carbon loading
2.0 mg cm-2 carbon loading
Pressure Gradient (Pa m-1)
Velocity of flowing gas (ms-1)
0.0
1.0×10^3
2.0×10^3
3.0×10^3
4.0×10^3
5.0×10^3
6.0×10^3
7.0×10^3
8.0×10^3
9.0×10^3
1.0×10^4
1.1×10^4
1.2×10^4
1.3×10^4
1.4×10^4
1.5×10^4
2.0×10^-4
4.0×10^-4
6.0×10^-4
8.0×10^-4
1.0×10^-3
1.2×10^-3
1.4×10^-3
1.6×10^-3
1.8×10^-3
2.0×10^-3

(e)

705

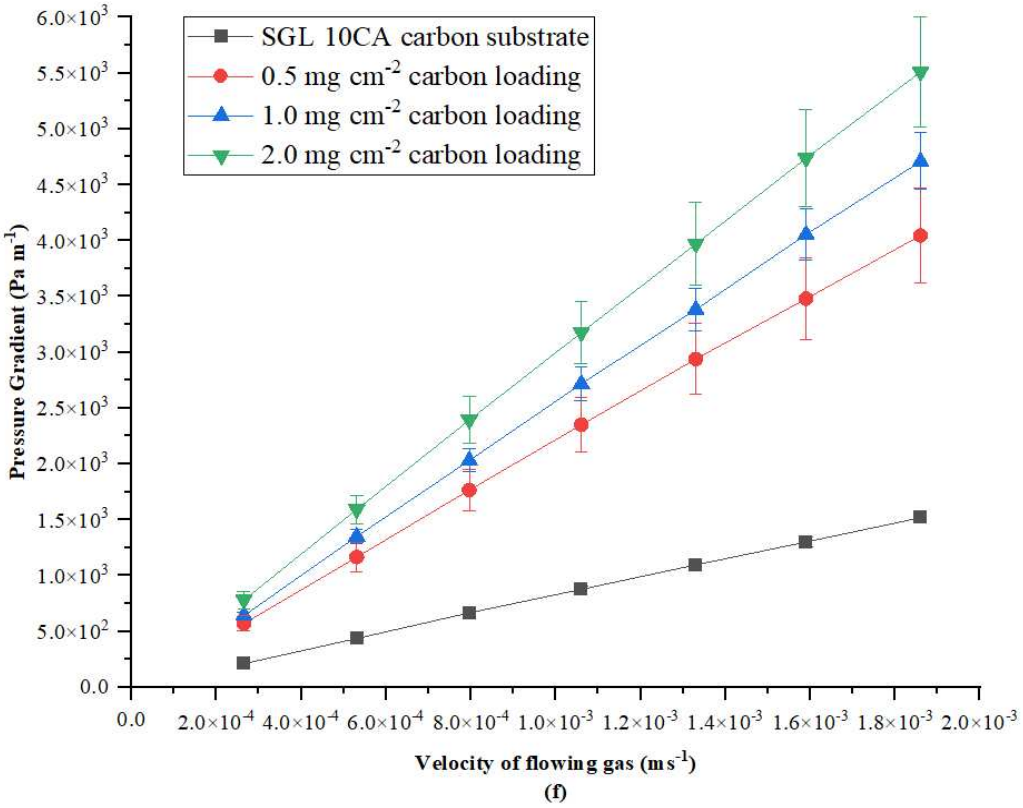

Figure F-1. Experimental data for the pressure gradient as a function of fluid velocity for (a-b) Toray-TGP-H 90, (c-d) SGL 35BA coat and (e-f) SGL 10CA coated with Vulcan XC-72R (a, c, e) and Ketjenblack EC-300J (b, d,f).

Table A-1. Through-plane gas permeability of the GDLs coated with Vulcan XC-72R and Ketjenblack EC-300J.

GDL substrate	**Permeability** $k \times 10^{-12}$ **m²**					
	Vulcan XC-72R			**Ketjenblack EC-300J**		
	0.5 mg cm-2	**1.0 mg cm-2**	**2.0 mg cm-2**	**0.5 mg cm-2**	**1.0 mg cm-2**	**2.0 mg cm-2**
Toray TGP-H-120	2.43 ± 0.58	0.29 ± 0.06	0.24 ± 0.04	1.48 ± 0.17	1.90 ± 0.82	2.82 ± 0.65
Toray	3.15 ± 0.91	0.40 ± 0.12	0.26 ± 0.03	1.51 ± 0.3	2.44 ± 0.94	2.98 ± 0.31

TGP-H-90						
SGL 35BA	15.1 ± 2.21	3.78 ± 0.81	0.89 ± 0.19	10.22 ± 2.34	11.64 ± 2.58	18.19 ± 2.30
SGL 10CA	7.99 ± 1.11	5.32 ± 0.54	3.39 ± 0.57	8.28 ± 0.88	7.15 ± 0.80	6.08 ± 0.58
SGL 10EA	4.43 ± 1.07	1.67 ± 0.40	1.09 ± 0.15	7.82 ± 2.18	6.20 ± 0.44	3.57 ± 0.67

711

712

713